Title

A Hepatitis C virus genotype 1b post-transplant isolate with high replication efficiency in cell culture and its adaptation to infectious virus production in vitro and in vivo

Short title

Infectious Hepatitis C virus genotype 1b isolate

Authors

Christian Heuss[1]†, Paul Rothhaar[1]†, Rani Burm[2], Ji-Young Lee[3], Uta Haselmann[3], Luisa J. Ströh[4], Philipp Ralfs[1], Ombretta Colasanti[1], Cong Si Tran[1], Noemi Schäfer[1], Paul Schnitzler[5], Uta Merle[6], Ralf Bartenschlager[3,7,8], Arvind H. Patel[9], Frederik Graw[10,11], Thomas Krey[4,12,13,14,15], Vibor Laketa[5,7], Philip Meuleman[2], Volker Lohmann[1,7*]

Affiliations

[1]Department of Infectious Diseases, Molecular Virology, Section virus-host interactions, Heidelberg University, Heidelberg, Germany.
[2]Laboratory of Liver Infectious Diseases, Ghent University, Gent, Belgium.
[3]Department of Infectious Diseases, Molecular Virology, Heidelberg University, Heidelberg, Germany.
[4]Institute of Virology, Hannover Medical School, Hannover, Germany.
[5]Department of Infectious Diseases Virology, University Hospital Heidelberg, Heidelberg, Germany.
[6]Department of Internal Medicine IV, University Hospital Heidelberg, Heidelberg, Germany.
[7]German Center for Infection Research, partner site Heidelberg, Heidelberg, Germany.
[8]Division Virus-Associated Carcinogenesis, Germany Cancer Research Center (DKFZ), Heidelberg, Germany.
[9]MRC-University of Glasgow Centre for Virus Research, Glasgow, UK.
[10]BioQuant – Center for Quantitative Biology, Heidelberg University, Heidelberg, Germany.
[11]Interdisciplinary Center for Scientific Computing, Heidelberg University, Heidelberg, Germany.
[12]Center of Structural and Cell Biology in Medicine, Institute of Biochemistry, University of Lübeck, Lübeck, Germany.
[13]Centre for Structural Systems Biology (CSSB), Hamburg, Germany.
[14]German Center for Infection Research (DZIF), Partner Site Hamburg-Lübeck-Borstel-Riems, Lübeck, Germany.
[15]Cluster of Excellence RESIST (EXC 2155), Hannover Medical School, Hannover, Germany.

† These authors contributed equally to this work.

* Corresponding author: Volker.Lohmann@med.uni-heidelberg.de

Abstract

Hepatitis C virus (HCV) is highly diverse and grouped into eight genotypes (gts). Infectious cell culture models are limited to a few subtypes, that do not include the highly prevalent gt1b, hampering the development of prophylactic vaccines. A consensus gt1b genome (termed GLT1) was generated from an HCV infected liver-transplanted patient. GLT1 replicated to an outstanding efficiency in Huh7 cells upon SEC14L2 expression, by use of replication enhancing mutations or with a previously developed inhibitor-based regimen. RNA replication levels almost reached JFH-1, but full-length genomes failed to produce detectable amounts of infectious virus. Long-term passaging led to the adaptation of a genome carrying 21 mutations and concomitant production of high levels of transmissible infectivity (GLT1cc). During the adaptation, GLT1 spread in the culture even in absence of detectable amounts of free virus, but cell-to-cell spreading efficiency was not higher as in other isolates like JFH-1. Mechanistically, genome replication and particle production efficiency were enhanced by adaptation, while cell entry competence of HCV pseudoparticles was not affected. Furthermore, GLT1cc retained the ability to replicate in human liver chimeric mice, which was critically dependent on a mutation in domain 3 of nonstructural protein NS5A. Over the course of infection, only one mutation in the surface glycoprotein E2 consistently reverted to wildtype, facilitating assembly in cell culture but potentially affecting CD81 interaction in vivo.

Overall, GLT1cc is the first efficient gt1b infectious cell culture model, paving the road to a rationale-based establishment of new infectious HCV isolates and represents an important novel tool for the development of prophylactic HCV vaccines.

Author summary

Chronic HCV infections remain an important global health issue, despite the availability of

64 highly efficient therapies. So far no protective vaccine is available, which is in part due to
65 the high divergence of HCV variants and the limited possibly to mirror this genetic diversity
66 in cell culture. It has been proven particularly difficult to grow infectious virus in cell
67 culture, requiring extensive adaptation with multiple mutations, which in turn affect
68 infectivity of the adapted variants in vivo. Here we have isolated a genotype 1b variant from
69 a very high titer serum of a patient after liver transplantation (German Liver Transplant 1,
70 GLT1), showing an outstanding genome replication efficiency in cultured hepatoma cells.
71 We were able to adapt this isolate to production of infectious virus, therefore generating the
72 first efficient full-replication cycle cell culture model for highly prevalent HCV genotype
73 1b. Despite multiple mutations required, adapted GLT1 was still infectious in vivo. GLT1
74 therefore is not only an important novel development facilitating future efforts in vaccine
75 development. It also provides novel perspectives towards our understanding how liver
76 transplantation drives the evolution of viral isolates with high replication capacity, which
77 might contribute to direct pathogenesis of HCV infection.
78
79

80 **Introduction**

81 Worldwide more than 71 million people are chronically infected with the Hepatitis C virus
82 (HCV) (1) resulting in a high risk to develop severe liver disease and hepatocellular
83 carcinoma (2). Despite the availability of highly efficient therapies based on direct-acting
84 antivirals (DAA) (3), the World Health Organization classified HCV infections as a public
85 health threat (4). HCV belongs to the genus *Hepacivirus* in the family *Flaviviridae.* Due to
86 its genetic heterogeneity, the virus is classified into eight genotypes that differ in their
87 nucleotide sequence by up to 30%, representing a major hurdle for the development of
88 prophylactic vaccines (5-8). Genotype 1, and the subtypes 1a and 1b, are most prevalent
89 worldwide (9). HCV is an enveloped positive-strand RNA virus, comprising a genome of
90 approximately 9600 nucleotides that encodes a single polyprotein flanked by two non-
91 translated regions. The polyprotein is processed by cellular and viral proteases into three
92 structural proteins (core, E1 and E2) and seven non-structural proteins (p7, NS2, NS3,
93 NS4A, NS4B, NS5A and NS5B). The structural proteins core (capsid) and E1/E2 (envelope
94 glycoproteins) are physical components of the virus particle. p7 is a viroporin important for
95 virus release and NS2 is part of the NS2-3 autoprotease and contains three N-terminal
96 transmembrane segments vital for virion morphogenesis. NS3, NS4A, NS4B, NS5A and
97 NS5B are essential and sufficient components of the viral replicase, all contributing to the
98 generation of membranous replication organelles designated the membranous web and
99 contributing to viral RNA synthesis, but also to virion assembly. NS3 harbors an N-terminal
100 protease activity responsible for the cleavage of all NS3-5B junctions with its co-factor
101 NS4A and a C-terminal helicase. NS4B is a key factor for the biogenesis of the membranous
102 web. NS5A is a phosphoprotein proposed as a key regulator of RNA replication
103 and assembly. NS5B is the viral RNA-dependent-RNA polymerase (RdRp) (reviewed in
104 (10)).

105 Even more than 30 years after the discovery of HCV, it remains challenging to replicate
106 patient-derived wildtype (WT) viral isolates in cultured cells. The first cell culture models
107 based on subgenomic gt1b replicons (prototype isolate Con1) in the HCC derived cell line
108 Huh7 revealed the need for replication enhancing mutations to obtain robust RNA
109 replication (11, 12). These mutations were also a prerequisite for the establishment of
110 replicons of almost all other genotypes (1a, 3a, 4a, 5a, 6a) (reviewed in (13)). The only
111 exception so far is the gt2a isolate JFH-1, which is capable of highly efficient RNA
112 replication in Huh7 (14). Meanwhile, the need for replication enhancing mutations has been
113 overcome to some extent. First, reconstitution of SEC14L2 expression, a lipid transport
114 protein expressed in human hepatocytes but not in Huh7, facilitated replication of WT
115 isolates of all genotypes (15), albeit with varying efficiency (16). Second, the identification
116 of the mechanisms underlying replication enhancing mutations in NS5A (prototype:
117 S2204I/R, referring to the amino acid position in the polyprotein of Con1) and NS5B
118 (R2884G) (Lohmann et al., 2003), allowed the development of an inhibitor regimen termed
119 PCi, based on the combined chemical inhibition of Phosphatidylinositol-4 kinase III alpha
120 (PI4KA) and Casein Kinase Ia (CKIα), enabling RNA replication of gt1b isolates by
121 compensating for the overexpression of PI4KA in HCC-derived cells, compared to human
122 hepatocytes (17).
123 The second and even more demanding hurdle relates to the difficulty in generating
124 infectious virus in cell culture. Since most initially identified replication enhancing
125 mutations impaired or abrogated virus production (18), resulting in attenuation in vivo (19),
126 it required the JFH-1 isolate to allow producing low amounts of infectious virus in cell
127 culture (20). However, here titer-enhancing mutations were necessary for robust virus
128 production (21) or chimeric genomes encoding the structural proteins, p7 and NS2 of
129 another gt2a isolate (J6, (22)), either entirely (J6/JFH-1, (23)) or in parts (JC1, (24)). Later,

130 a gt1a genome containing five replication and titer enhancing mutations was established,
131 generating infectious virus with limited efficiency (25). Meanwhile, additional genomes
132 capable of infectious virus production based on gt1a, gt2, gt3a and gt6a have been generated
133 (reviewed in (26)). Most of them were obtained using JFH-1-based chimeras as a starting
134 point, building on repetitive passaging and recloning cycles, finally resulting in numerous
135 replication- and titer-enhancing mutations (reviewed in (26)). However, even though gt1b
136 requires only one replication enhancing mutation and is effectively stimulated by SEC14L2
137 expression or PCi treatment (16, 17), so far no efficient cell culture model supporting the
138 entire replication cycle is available.
139 This study aimed at establishing a gt1b isolate capable of efficient virus production in cell
140 culture. Starting from a high titer serum of a post-transplant patient, we generated a
141 consensus genome termed GLT1 with RNA replication capacity close to JFH-1. Infectious
142 virus production required more than a year with a total of 118 cell passages and 27
143 supernatant transfers. The cloned GLT1cc genome contains 21 mutations, facilitating
144 efficient virus production and spread, still retaining infectivity in vivo. GLT1cc therefore
145 closes an important gap in the availability of full-replication cycle models of all major HCV
146 genotypes and might greatly facilitate the development of a protective vaccine.
147

148 **Results**

149 **Generation of GLT1 and analysis of RNA replication efficiency in cell culture**

150 We recently established a drug regimen based on pharmacological inhibition of PI4KA and
151 CKIα (designated PCi) enhancing RNA replication of gt1b WT isolates by approximately
152 100-fold, allowing infection of Huh7 hepatoma cells with several patient-derived gt1b sera
153 (17). One serum with an exceptionally high viral load (>100,000,000 IU/ml) gave rise to a
154 particularly strong increase in RNA replication upon PCi treatment (17), indicating a viral

155 isolate with exceptional replication efficiency. We therefore PCR-amplified the viral
156 genomic sequences from infected Huh7 cells and generated a consensus sequence based on
157 direct sequencing of the PCR products. In case of equivocal sequencing data, which affected
158 the amino acid sequence only at two positions (aa849 in NS2 and 2760 in NS5B), we opted
159 to incorporate the respective variant with higher frequency. This novel gt1b isolate was
160 termed German Liver Transplant 1 (GLT1), since the serum was obtained from a patient
161 after liver transplantation. Alignment of the GLT1 coding sequence with a general gt1b
162 consensus sequence (Fig. 1A, upper panel) or the widely used gt1b isolate Con1 (11) (Fig.
163 1A, lower panel) revealed 95% and 94% identity, respectively. A phylogenetic tree of 358
164 available gt1b full-length genome sequences further demonstrated that the GLT1 isolate is
165 located in one of the main branches of this subtype (Fig. 1B).
166 We next aimed to characterize GLT1 in terms of its RNA replication efficiency as well as
167 its ability to produce infectious virus in cell culture. To this end we generated a synthetic
168 consensus sequence for construction of a subgenomic reporter replicon and a full-length
169 genome. We first determined RNA replication efficiency in comparison to isolates widely
170 used in the field, representing experimental gold-standards so far (Fig. 1C-F, Fig. S1-S3):
171 JFH-1 (gt2a), the only HCV isolate replicating efficiently in cell culture without any
172 modification, and Con1 (gt1b) (11), a prototype isolate more closely representing the
173 phenotype of all other cloned HCV isolates, requiring either PCi treatment (17), SEC14L2
174 expression (Fig. S1A; (15)) or replication enhancing mutations for efficient RNA replication
175 (12, 27, 28). To assess RNA replication efficiency, we transfected luciferase reporter
176 replicons (Fig. S1B) of the three isolates into Huh7 cells (Fig. S2) and two highly permissive
177 Huh7 subclones, Huh7-Lunet (Fig. 1C-F, S1C, (17)) and Huh7.5 (Fig. S3; (29)),
178 implementing all replication enhancing conditions accessible so far and using firefly
179 luciferase activity as a quantitative measure. While GLT1 replication was only slightly

180 increased in naïve Huh7-Lunet cells compared to Con1 (Fig. 1C,D, black lines), stimulation
181 by PCi treatment was far more pronounced (Fig. 1C, green lines), almost reaching JFH-1
182 levels at 72 h after transfection. A similar increase was obtained by ectopic expression of
183 SEC14L2 (Fig. 1D,E, red lines; Fig. S1A). Combination with PCi treatment had a slightly
184 additive effect on Con1 and GLT1, but confirmed the overall 100-fold higher replication
185 efficiency of GLT1. JFH-1 replication was not affected by SEC14L2 expression and slightly
186 reduced upon PCi treatment, due to its different requirement for PI4P (17).
187 We further compared the impact of a set of well characterized replication enhancing
188 mutations on Con1 and GLT1 (Fig. 1F, (28)). Here, replication enhancement of GLT1 was
189 the highest for a mutation in NS4B (mut4B, K1846T), following overall the same pattern
190 as Con1, but again with 100-fold higher efficiency reaching a similar level as SEC14L2
191 combined with PCi (Fig. 1E, blue lines). Combinations of adaptive mutations with
192 SEC14L2 expression did not further increase replication levels of the mut4B variant (Fig.
193 S1C). Similar results were obtained in Huh7 (Fig. S2) and Huh7.5 cells (Fig. S3), albeit
194 with overall slightly lower efficiency.
195 In conclusion, we identified and cloned a novel genotype 1b isolate (GLT1) from a liver
196 transplant patient with about 100-fold higher replication efficiency than the closely related
197 prototype isolate Con1. Efficient GLT1 wildtype replication in Huh7-derived cells required
198 support by expression of SEC14L2, or by a previously established inhibitor cocktail, with
199 some additive effects. A replication enhancing mutation in NS4B resulted in highest
200 replication levels
201
202 **Morphology of the replication organelles of GLT1**
203 We next explored whether changes in the ultrastructure of replication organelles might
204 explain the outstanding RNA replication competence of GLT1. This so-called membranous

205 web mainly consists of double membrane vesicles (DMVs) with an average diameter of ca.
206 200 nm (30, 31). We first analyzed DMV abundance and size in cells transiently transfected
207 with GLT1 replicons under all conditions providing sufficient replication efficiency for
208 thorough quantification (PCi treatment, SEC14L2 expression or replication enhancing
209 mutation mut4B; Fig. 2). We used a reporter system based on the expression of GFP with a
210 nuclear translocation signal fused to the membrane anchor of MAVS (MAVS-GFP-NLS,
211 (17, 32)) harboring the NS3-4A cleavage site. This allowed for the identification of HCV
212 positive cells by nuclear GFP localization in correlative light and electron microscopy
213 (CLEM). The DMV abundance was very variable due to the random choice of areas, but
214 overall comparable (Fig. 2A). The average DMV diameter ranged from 129-145 nm, which
215 was relatively small compared to Con1 and JFH-1 WT (180-200 nm (17, 30)). To exclude
216 the impact of the replication enhancing conditions, we expressed GLT1 NS3-5B WT in
217 naïve Huh7-Lunet T7 cells and found similar DMV diameters, which were also not affected
218 by SEC14L2 expression (141 nm and 144 nm, respectively, Fig. S4A-C). Since reduced
219 DMV diameters were previously associated with reduced PI4P concentrations (17, 31), we
220 compared the level of PI4KA activation by expression of NS3-5B of JFH-1, Con1 and
221 GLT1 (Fig. S4D,E). Indeed, PI4P concentrations in HCV positive cells were significantly
222 reduced in case of GLT1, pointing to a reduced level of PI4KA activation, similar to a class
223 of replication enhancing mutations (mut5A and mut5B; (17)). The reduced level of PI4KA
224 activation by GLT1 is therefore the likely cause of the observed changes in DMV phenotype
225 and the potential reason of the increased replication of GLT1 compared to Con1 WT in
226 naïve Huh7 cells (Fig. 1C, black lines).
227 In sum, replication organelles of GLT1 WT contained smaller DMVs compared to other
228 HCV isolates, in line with a reduced capacity to activate PI4KA. This might explain in part
229 the higher replication capacity compared to related isolates.

230

231 **Full-length GLT1 requires extensive adaptation to generate transmissible infectivity**

232 Next, we assessed if the GLT1 full-length genome was capable of producing infectious virus
233 particles in Huh7 cells. We again used either PCi treatment or ectopic SEC14L2 expression
234 to stimulate WT virus replication, including Con1 as a reference gt1b isolate. In addition,
235 we used GLT1-mut4B since the K1846T mutation in Con1, in contrast to other major
236 adaptive mutations, is known not to interfere with infectious virion production (18, 19). As
237 a reference for efficient viral replication and virion release, we included the gt2 chimeric
238 J6CF/JFH-1 genome, called JC1 (24). In vitro transcribed full-length genomes were
239 transfected into Huh7-Lunet cells and the intra- or extracellular amount of viral core protein
240 was quantified as a correlate of RNA replication efficiency and virion production,
241 respectively (Fig. 3A). Differences in intracellular core levels for the different variants and
242 conditions were consistent with the data of luciferase reporter replicons (Fig. 1C-F).
243 Extracellular core levels were by far the highest in case of JC1 and almost undetectable for
244 Con1, as expected. In case of GLT1 WT, high intracellular core protein levels correlated
245 with increase in the extracellular core protein for PCi treatment and SEC14L2 expression,
246 as well as for mut4B, but remained 100-fold lower than JC1. A similar increase was
247 observed in Huh7.5 cells, albeit with slightly lower efficiency (Fig. S5A). The level of
248 extracellular core protein did not increase by combined PCi treatment and SEC14L2
249 expression (Fig. 3A), nor by the generation of a chimeric gt1b genome containing the
250 structural proteins and parts of NS2 of Con1 and the replication module of GLT1
251 (Con1/C3GLT1, Fig. S5B). To assess the presence of infectious virus, we used Huh7-Lunet
252 CD81 cells stably expressing the MAVS-GFP-NLS reporter (*17*) allowing for a sensitive
253 detection of infection events in living cells. For transfer of supernatants of Con1 and GLT1

254 WT we further expressed SEC14L2 in the recipient cell line. However, no infection events
255 were detectable from supernatants at 72 h after transfection except for JC1 (Fig. 3A,B).
256 Strong increase of infectious virus levels for JFH-1 and other isolates was achieved by
257 passaging of transfected cells, followed by supernatant passaging, resulting in the
258 accumulation of titer-enhancing mutations (26). We tried this approach also for GLT1, using
259 the most promising conditions (SEC14L2 expression and GLT1-mut4B) and including
260 Con1 as a control (Fig. 3C). Huh7-Lunet cells with or without SEC14L2 expression were
261 transfected with the respective HCV variants and passaged twice a week. The status of each
262 culture was monitored using the extracellular core protein level (Fig. 3C) as well as the GFP
263 localization. The level of extracellular core protein constantly declined in case of Con1 and
264 GLT1 WT in SEC14L2 expressing cells and finally fell below the limit of detection at p5
265 and p15, respectively. Con1/C3GLT1 performed slightly better, still amounts of secreted
266 core protein continuously declined and the passaging was stopped after p21 since no
267 detectable amounts of infectious virus were found after transfer of supernatant (Fig. S5C).
268 GLT1-mut4B led to consistent secretion of core protein and transfer of concentrated
269 supernatant of passage number 29 finally resulted in some small clusters of positive cells
270 representing infection events (Fig. 3D). The initially low number of positive cells increased
271 upon passaging and we continued to transfer pure or concentrated supernatants after 3-5 cell
272 passages to naïve reporter cells (Fig. 3E). After 8 supernatant transfers and a total of 64 cell
273 passages (p64.8, Fig. 3E), the first infection events upon transfer of pure supernatant were
274 obtained (Fig. 3E). Interestingly, the initial number of infection events after each
275 supernatant transfer did not change dramatically, but the velocity of spread within the
276 culture, estimated by the number of GFP positive nuclei, increased rapidly within a few
277 passages up to approximately 80% positive cells (Fig. 3E), consistent with the dynamics of
278 core-secretion (red lines). Since continuous passaging did not substantially increase the

279 initial number of infected cells after supernatant transfer, nor the number of passages
280 required to reach 80% positive cells further decreased, we stopped the experiment after 27
281 supernatant passages, including a total number of 118 cell passages (p118.27).
282 To identify potential titer enhancing mutations, we determined the consensus sequence of
283 the viral quasispecies by direct sequencing of PCR products after the first passage of
284 concentrated supernatant (p32.1), the first successful passage of pure supernatant (p64.8)
285 and at the endpoint of the experiment (p118.27) (Fig. 3F). The number of conserved
286 mutations successively increased to 19 at p118.27, whereas K1846T was maintained,
287 resulting in a total of 20 deviations compared to GLT1 WT. Mutations were spread over the
288 entire polyprotein with one mutation in the core protein (I30T) four in the glycoproteins E1
289 and E2 (H202Y / Q434R / F437L / V719L), two in NS2 (I888V / V899A), two in NS3
290 (V1074I / A1226G), two in NS4B (S1827T / I1834L), five in NS5A (R2080K / N2152S /
291 V2340A / S2341P / Y2385H) and three in NS5B (N2561T / Q2603K / C2864F). Due to this
292 large number and the incremental increases in efficiency over the course of passaging, we
293 opted to not study the titer enhancing effects of individual mutations. Instead, we generated
294 a consensus clone of the dominant viral sequence found at p118.27, which we termed GLT1-
295 20M. Transfection of in vitro transcribed homogenous GLT1-20M resulted in $1.5x10^2$
296 TCID50 per ml compared to $3x10^1$ detected in the heterogenous population of supernatant
297 p118.27 and $1x10^4$ for JC1 (Fig. 3G).
298 In conclusion, full-length GLT1, neither wildtype nor the mut4B genome, produced
299 efficient levels of infectious virus in cell culture. However, after continuous rounds of cell
300 and supernatant passages the viral genome acquired 19 potential titer enhancing mutations,
301 generating a low but detectable level of transmissible virus.
302

303 **Characterization of GLT1 transmission mechanisms**

304 Since GLT1 showed a rapid increase in the number of HCV positive cells (up to 80%) after
305 a few passages, despite the low amounts of free virus in the supernatant, we aimed to further
306 characterize the modes of transmission. In a continuous culture, new positive cells can occur
307 by division of infected cells, by transmission of free virus or by cell-to-cell spread (33, 34).
308 To allow quantification of transmission events, we established a co-culturing assay based
309 on co-seeding of HCV positive cultures of MAVS-GFP-NLS cells with naïve cells
310 harboring MAVS-mCherry-NLS in a ratio of 1:5. Therefore, cells with nuclear GFP signal
311 could be classified as "donor", whereas cells with nuclear mCherry signal could be
312 interpreted as "recipient", based on automated image analysis of whole wells at 24, 48 and
313 72 h after seeding (Fig. 4A). Donor cultures were either chosen from the critical points of
314 the passaging experiment (p32.1, p64.8 and p118.27, Fig. 3E), or after transfection of in
315 vitro transcripts of defined variants (GLT-20M, JC1). Interestingly, the capacity of GLT1
316 to spread in cell culture increased with continuous passaging, similarly to the appearance of
317 free transmissible virus (Fig. 4B). However, the consensus genome GLT1-20M spread to
318 naïve cells nearly as efficiently and with similar kinetics as JC1 (Fig. 4B), despite the far
319 lower titers (Fig. 3G). The ability of viral spread for both genomes was dependent on the
320 presence of CD81 as the co-culture with Huh7-Lunet CD81N cells, lacking CD81
321 expression (34, 35) gave rise to less than 1% transmission rates (Fig. 4C). To differentiate
322 between cell free transmission and cell-to-cell spread we next aimed to block cell free
323 transmission by the addition of neutralizing antibodies, comparing GLT1-20M with JC1
324 and the cell culture adapted gt3a isolate DBN3acc (36), generating similar titers as GLT1-
325 20M (Fig. S6A). We chose two different broadly neutralizing anti-E2 antibodies efficiently
326 blocking infection: AP33 (37, 38) and an equimolar mixture of Fab fragments derived from
327 the two potent neutralizing antibodies AR3C (39) and HC84.1 (40) termed Fab mix. Indeed

328 both antibodies blocked infection of JC1 and DBN3acc with similar efficiency, preventing
329 80-90% of infection events (Fig. 4D). For GLT1-20M, infection was undetectable upon
330 AP33 treatment, whereas, Fab mix was far less efficient under these conditions (Fig. 4D).
331 In the co-culture setting, the antibodies were applied upon co-seeding of the cells and
332 infection was evaluated 72 h later. Interestingly, the presence of neutralizing antibodies
333 suppressed less than 50% of infection events in case of JC1, 30-40% in case of DBN3acc
334 and inhibition ranged from 40% (Fab mix) to 80% (AP33) for GLT1-20M, in line with the
335 varying neutralization capacity (Fig. 4E). Overall, these data suggested that most of the
336 GLT1-20M transmission events were dependent on E2 and could be blocked by anti-E2
337 neutralizing antibodies, arguing against a higher cell-to-cell spread efficiency compared to
338 that of JC1 or DBN3acc.
339 Analysis of the spatial distribution at single cell resolution of donor and recipient cells
340 confirmed the varying impact of the neutralizing antibodies for JC1 and GLT1-20M.
341 Despite similar cell densities, donor cells for GLT1-20M had on average a considerably
342 lower frequency of recipient cells in their direct surrounding than donor cells for JC1 (Fig.
343 4F). Furthermore, only 24% of all donor cells had at least one recipient cell within a radius
344 of 50 μm, in contrast to 65% for JC1 (Fig. 4G). Supplementation of antibodies, especially
345 AP33, reduced the frequency of these growing donor foci for GLT1-20M by nearly 50%,
346 while there was no effect for JC1 (Fig. 4G). As a result of the strong impact of the antibodies
347 on GLT1-20M spread, the median distance between a donor cell and the next recipient cell
348 was strongly increased (Fig. S6B) in contrast to JC1, which generally experienced smaller
349 distances between donor and recipient cells independent of the treatment conditions (Fig.
350 S6C). Thus, also the local analysis showed that GLT1-20M had a lower transmission
351 capacity and was more effectively blocked by neutralizing antibodies than JC1. However, a
352 clear limitation of this analysis was the undefined time-lapse between transmission event

353 and nuclear transfer of mCherry-NLS (16 h-48 h, Fig. S7A,B,E, Movie S1-S3), as well as
354 the motility of the donor and recipient cells (Fig. S7C, Movie S4) and other unexpected
355 events like the death of donor cells (Fig S7D, Movie S5). Therefore, a cell-to-cell contact
356 at the time of infection could not be formally excluded in some of the analyzed infection
357 events.
358 In summary, acquired adaptive mutations for GLT1-20M mediated the ability to produce
359 infectious virus and to spread in cell culture. Detailed analysis of the viral accessibility
360 towards broadly neutralizing antibodies during viral spread did not support a higher cell-to-
361 cell spreading efficiency of GLT1-20M compared to JC1 or DBN3acc.
362
363 **Generation of GLT1cc**
364 In search for further ways to improve the efficiency of GLT1-20M in terms of viral titers,
365 we analyzed the quasispecies of p118.27 to identify minor variants with promising potential,
366 by sequencing a panel of individual cloned PCR products (Fig. S8A). Indeed, three of five
367 subclones contained the mutation N2415S, located at the P5 position of the NS5A-NS5B
368 cleavage site of NS3-4A. Since a previous study found a titer enhancing mutation at P3,
369 which was shown to slow down processing of NS5A-NS5B (21) and mutations at this or at
370 neighboring positions were also found in almost all cell culture adapted variants of other
371 isolates (26), we reasoned that N2415S might have a titer enhancing effect in case of GLT1
372 as well. Interestingly, N2415S already increased the amount of secreted infectivity to low
373 but detectable levels in case of GLT1-mut4B and enhanced titers of GLT1-20M by about
374 10-fold in every single experiment (Fig. 5A). We thereby reached TCID50 values for GLT1-
375 20M+N2415S around 10-fold below JC1 in Huh7-Lunet cells. For Huh7.5 cells, titers were
376 substantially lower (Fig. S8B), likely due to the reduced replication efficiency of gt1b in
377 this subclone (Fig. 1 compared to Fig. S3). The levels of secreted core protein and HCV

378 genomic RNA were not substantially increased by addition of N2415S (Fig. 5B,C), but the
379 number of infected cells in a bulk culture infection (Fig. 5D). At this point we decided to
380 stop further attempts to increase GLT1 titers and therefore termed GLT1-20M+N2415 as
381 GLT1cc, in accordance with previous studies (23, 26, 41).
382 In summary, combining a replication enhancing mutation in NS4B with 19 conserved
383 changes acquired during passaging and one intentionally added mutation at the C-terminus
384 of NS5A dramatically enhanced the efficiency of infectious virus production by the GLT1
385 isolate. This variant was designated GLT1cc.
386
387 **Mechanisms of titer enhancement**
388 The changes acquired upon passaging were widespread across all viral proteins except p7
389 and NS4A (Fig. 6A). Some variants were found in several published isolates, others were
390 unique. We therefore addressed the basic mechanisms underlying the improved efficiency
391 of infectious virus production of GLT1cc by comparing RNA replication efficiency in a
392 subgenomic replicon, entry efficiency using retroviral pseudoparticles decorated with the
393 HCV glycoproteins (HCVpp) (42) and virus production in a JFH-1-based chimeric construct
394 (24, 43) (Fig. 6B-D). Since most mutations were found in the replicase proteins, we indeed
395 found a clear increase in RNA replication kinetics for GLT1-20M and GLT1cc compared
396 to GLT1-mut4B, suggesting that titer enhancement in part might be due to higher RNA
397 replication levels (Fig. 6B). Still, this did not exclude that changes in the NS proteins might
398 further contribute to virion production by their reported functions in viral assembly
399 (reviewed in (44)). Interestingly, when we replaced the structural protein coding region in
400 the chimeric reporter virus genome of JCN2A (43) by the GLT1 counterparts, RNA
401 replication was not affected, but production of infectivity was reduced to the level of the
402 negative control ΔE1E2 (Fig. 6D). This was not unexpected, since such intergenotypic

403 chimeras often suffer from incompatibility of replication and assembly modules (24, 45),
404 requiring further adaptation. However, the mutations found in GLT1cc partially rescued
405 assembly of the chimeric genome, suggesting that these changes indeed facilitate the
406 morphogenesis of infectious virions (Fig. 6D). In contrast, entry efficiency of HCVpp was
407 comparable between GLT1 and GLT1cc and similar to Con1 in Huh7-Lunet CD81 cells
408 (Fig. 6C). Due to the expected incremental contribution of individual mutations and the
409 complexity of possible combinations, we did not further try to evaluate whether or not
410 individual changes contributed to the phenotype.
411

412 **GLT1 replication in human liver chimeric mice**

413 Finally, we evaluated the infectivity of GLT1 WT, GLT1-mut4B, GLT1-20M and GLT1cc
414 in vivo, using homozygous uPA+/+-SCID mice transplanted with primary human
415 hepatocytes, rendering them permissive for HCV infection (46). In case of GLT1 WT, we
416 used the high-titer post-transplant patient serum as inoculum, due to its homogenous
417 consensus sequence and the lack of efficient virus production in cell culture. Indeed, three
418 out of three mice got infected and showed a high titer viremia for several weeks, with
419 slightly different courses, which were within the regular variations found in this model (Fig.
420 7A). We confirmed the HCV consensus sequence in total liver RNA of one of the mice
421 sacrificed 8 weeks post infection by direct sequencing of RT-PCR products covering the
422 whole HCV coding sequences to be identical with GLT1. Only at two positions (K1052R
423 in NS3 and R1649K in NS4A) previous minor variants present in the inoculum became
424 dominant (Fig. 7B, S9). This result confirmed that GLT1 WT was infectious in vivo,
425 supporting the entire viral replication cycle, albeit not generating detectable infectivity in
426 cell culture.

427 Next, we aimed for a comparison of GLT1-mut4B, GLT1-20M and GLT1cc. Since
428 infectious virus was not detectable in cell culture for GLT1-mut4B, we used the same
429 amounts of 100-fold concentrated supernatants for the intrasplenical infection of three mice
430 each (Fig. 7C). For GLT1-mut4B, one mouse got infected and reached a continuously high
431 titer, whereas one mouse died prior to the first blood withdrawal and one remained
432 uninfected (Fig. 7C, left panel), likely due to the low input titer (see Fig. 5). We found no
433 additional conserved mutations upon sequencing of the entire coding region amplified from
434 the serum of mouse 1 at week 6. This result demonstrated that the replication enhancing
435 mutation K1846T did not interfere with infectivity in vivo, as previously demonstrated for
436 the Con1 isolate (18). In contrast, all three mice infected with GLT1-20M reached only a
437 very transient viremia with titers close to the limit of detection, suggesting that the
438 accumulation of mutations required for titer enhancement in cell culture interfered with
439 replication in vivo (Fig. 7C, middle panel). This result was consistent with the lack of reports
440 of replication of any of the highly efficient HCVcc models in vivo, except those based on
441 JFH-1 (26) and gt1a H77S.2 (47), initiating a low titer transient viremia in human liver
442 chimeric mice. Surprisingly, in case of GLT1cc two mice got productively infected,
443 reaching titers similar to GLT1-mut4B, while again one mouse died early. This result argued
444 for a restoration of in vivo infectivity by the N2415S mutation. Determining the HCV
445 consensus sequence in the serum of both mice revealed a reversion at position 437 back to
446 the GLT1 WT sequence in both cases. The dominant HCV species in mouse 2 had no further
447 changes compared to GLT1cc, whereas mouse 1 had three additional conserved mutations.
448 This result demonstrated, that GLT1cc indeed is infectious in vivo. Introducing the
449 reversion at position 437 in GLT1cc revealed a negative effect on infectivity in hepatoma
450 cells (Fig. 7E). This indicates that the F437L mutation acquired already early upon

451 passaging in cell culture (Fig. 3F) is a titer enhancing mutation seemingly having a negative
452 impact in vivo and therefore reverting back to the GLT1 WT sequence.
453 Taken together, GLT1cc is the first viral isolate of a major genotype capable of efficient
454 replication and infectious virus production in cell culture combined with in vivo infectivity.
455

456 **Discussion**

457 In this study we have identified a novel gt1b WT isolate with highly efficient RNA
458 replication in cell culture and developed the first gt1b full-lifecycle cell culture system upon
459 adaptation by serial passaging, generating virions infectious in cell culture and in vivo.
460 Therefore, GLT1 is unique and paradigm breaking in several aspects.
461 The isolate was identified in a patient serum after two liver transplantations due to its ability
462 to infect and replicate efficiently in hepatoma cells upon PCi treatment (17). It is tempting
463 to speculate that this clinical background contributes to its outstanding replication capacity,
464 as it was discussed for JFH-1, isolated from an HCV patient with fulminant hepatitis (20)
465 and as it was the case for the gt1a TN strain, again from a fulminant hepatitis C patient,
466 which build the basis for the highly efficient TNcc clone (48). However, other isolates from
467 post-transplant sera, fulminant or acute hepatitis C did not replicate remarkably well in cell
468 culture or needed a series of adaptive mutations (e.g. JFH-2 (49), BHCV1 (50), NC1 (51)).
469 The ability to analyze replication of WT isolates in regular cell culture has only recently
470 been gained, either by expression of SEC14L2, a lipid transport protein expressed in PHH
471 but absent in Huh7 cells (15) or by PCi treatment, compensating for overexpression of the
472 lipid kinase PI4KA in Huh7 cells, mimicking the mechanism of replication enhancing
473 mutations in NS5A and NS5B (17). Therefore systematic studies on multiple WT isolates
474 like JFH-2, BHCV1 or NC1 are still missing but now are in reach. Still, PCi is only efficient
475 for gt1b isolates, since all other genotypes are restricted by additional unknown mechanisms

476 (17). SEC14L2 in contrast acts pangenotypically in selectable models (15), but has limited
477 stimulatory capacity beyond gt1 for cloned reporter replicons (16). Nevertheless, the fact
478 that GLT1 and Con1 RNA replication was elevated by both measures to a similar extent,
479 comparable to replication enhancing mutations, suggests that all methods reflect the true
480 replication capacity of an HCV isolate, at least within gt1b. This should encourage future
481 studies on the contribution of HCV fitness to persistence and pathogenesis, e.g. by
482 phenotypic analysis of isolates before and after liver transplantation. It will furthermore be
483 interesting to understand the determinants of the outstanding replication efficiency of GLT1,
484 e.g. by generating intergenotypic chimeras, as in case of JFH-1 (52).
485 While our understanding of factors limiting HCV RNA replication in cell culture and ways
486 to overcome it has tremendously increased in the last years, it is still technically challenging
487 to generate infectious virus from cloned isolates. Most systems available so far are based on
488 the replicase of gt2a JFH-1, albeit also here the genome has to be adapted to efficient virus
489 production, either by titer-enhancing mutations obtained upon passaging or by using the
490 structural proteins of the gt2a isolate J6 (see Ramirez and Bukh for recent comprehensive
491 review (26)). Since replication enhancing mutations have been shown to impair the
492 production of infectious virions to various extent (18, 19), the establishment of infectious
493 cell culture models for isolates apart from JFH-1 was very difficult and required tremendous
494 efforts. So far they have been established for gt1a, gt2a, gt2b, gt3a and gt6a, with varying
495 efficiency, requiring up to 20 mutations for efficient virus production (reviewed in (26)),
496 but no efficient gt1b isolate is available. Several in vivo infectious gt1b WT isolates have
497 been generated, including Con1 (19), which was the basis for the first efficient RNA
498 replication model (11). Indeed, by using an assembly neutral replication enhancing mutation
499 in NS4B (mut4B, K1846T), it was possible to show in principle the production of infectious
500 Con1 virus in cell culture and the infectivity of the virions in vivo, using the human liver

501 chimeric mice (18). However, virus could only be produced in very low amounts early after
502 transfection, suggesting the exclusive packaging of input-RNA; the virus did not spread in
503 culture and could not be further improved upon passaging. In case of GLT1, we used the
504 same mutation and also tried passaging of the WT isolate in SEC14L2 expressing cells, but
505 this time succeeded with mut4B and continuous passaging of cells and supernatants for
506 about one year. It is still not clear, why it was so difficult to generate an efficient gt1b
507 infectious cell culture system, but a striking observation was the fast increase of infected
508 cell numbers after supernatant transfer upon cell passaging, even in absence of detectable
509 amounts of free infectious virus (Fig. 3E). Cell-to-cell transmission, which appeared a
510 reasonable explanation, is a well-established phenomenon for HCV, defined as infection
511 events that cannot be blocked by neutralizing antibodies (34, 53). We established a co-
512 culture model, allowing image based analysis of transmission events, to understand whether
513 GLT1 is particularly efficient in cell-to-cell spread, but found no evidence supporting this
514 hypothesis. On the one hand, efficiency of spread in this model correlated with production
515 of infectious virus over the course of serial passaging. On the other hand, the spread of JC1
516 and DBN3acc, which were used for comparison, was less affected by the presence of
517 neutralizing antibodies than GLT1. These data suggest that cell-to-cell spread generally
518 represents an important transmission mechanism for HCV in cell culture, but still requires
519 the full assembly of infectious virus.
520 A total of 21 mutations were required to obtain GLT1cc from GLT1 WT. Since we only
521 took three snapshots of the consensus sequence at different stages of passaging, with 6-7
522 mutations acquired at each step, it is not clear, whether all changes were of functional
523 relevance. Due to the potentially incremental phenotypes expected from individual
524 mutations we refrained from a detailed analysis and instead analyzed the whole replicase
525 and the structural protein coding region separately for changes in RNA replication

526 efficiency and entry/assembly, respectively. The substantial stimulation of RNA replication
527 of GLT1-20M/GLT1cc was unexpected given the already high replication capacity of
528 GLT1-mut4B. However, it strengthens our assumption of robust RNA synthesis as a major
529 bottleneck for HCVcc production in Huh7 cells. Although direct contributions to assembly
530 have been reported for all NS proteins, it therefore seems likely that most of the mutations
531 in the NS3-5B region rather contribute to RNA synthesis, except those in domain 3 of NS5A
532 (44). Mutations in NS3/4A protease/helicase (Fig. 8C,D) and NS5B polymerase (Fig. 8F)
533 are key candidates mediating this phenotype, since they are located within the protein and
534 in part close to the active centers. In case of JFH-1, helicase and polymerase have indeed
535 been shown to underlie the outstanding replication efficiency of this isolate (52) and
536 mutation A1226G was also found in adapted gt1a isolate TNcc (48). Mutations in the
537 structured domain 1 of NS5A (Fig. 8E) are localized at the surface of the protein and rather
538 do not contribute to the different dimeric isoforms reported (Fig. S10). Their involvement
539 in RNA replication enhancement seems still plausible, but given the multitude of functions
540 of NS5A they might also contribute to assembly (54). In contrast, domain 3 of NS5A is a
541 key factor in virus assembly, due to its interaction with core (55), that results in the
542 recruitment of NS5A to lipid droplets (56) mediated by CKII dependent phosphorylation of
543 serine residues in this domain (55, 57). In case of GLT1cc, N2415S, located very close to
544 the NS5A-NS5B cleavage site, was particular striking, since it not only had a clear titer-
545 enhancing effect in cell culture, but furthermore rescued the low infectivity of GLT-20M in
546 vivo. A mutation in this region is found in almost all cell culture adapted viruses across
547 genotypes (26). In case of adapted JFH-1 it was shown that V2440L (corresponding to
548 position 2417 in GLT1) reduced NS5A-NS5B cleavage kinetics and thereby promoted virus
549 assembly (21). However, the mutation partially reverted to WT in human liver chimeric
550 mice (21), suggesting rather a cell culture specific function. Since N2415S even rescued the

551 in vivo replication capability of GLT1-20M and generated a potential phospho-acceptor
552 site, phosphorylation might be an attractive alternative mechanism (55, 57).
553 NS2 is another key factor of HCV assembly and particularly TMD3, where we found two
554 mutations (Fig. 8B), has been identified as a key component (58). Although this region was
555 not included in the chimeric construct we used to study assembly (C3, (24)), a contribution
556 to virus morphogenesis of GLT1cc appears possible. Among the other mutations
557 contributing to the increased assembly efficiency we observed for the GLT1cc/C3JFH-1
558 chimera, F437L is particularly interesting (Fig. 8A). On the one hand it appeared very early
559 in the passaging process and reversion to WT indeed reduced cell culture titers by about 10-
560 fold. On the other hand it was the only position reverting to WT in both infected human
561 liver chimeric mice, suggesting deleterious effects in vivo. F437L is located within Epitope
562 II, also named AS434, spanning from residue 428 to 446, which is overall highly conserved
563 among HCV genotypes (40, 59). An aromatic residue at position 437 is conserved through
564 all genotypes (59) and distinct mutations implying a reduction of the side chain
565 hydrophobicity at this position reduce binding to CD81 (40), thereby leading to a severe
566 viral entry defect (60) and a reduction in virus fitness (40). Residue 437 is further part of a
567 structurally conserved 1.5 alpha-helical turn (residue 437-442) in E2 and a mutation in this
568 motif has been proposed to lead to escape from neutralization by HC-84-related antibodies
569 targeting this region (40). F437L might therefore also be responsible for the reduced
570 neutralizing efficiency of the Fab mix observed for GLT1. The titer-enhancing effect we
571 observed for GLT1 might still be due to enhanced virion assembly or release efficiency.
572 Since we used cell lines with ectopic, saturating expression of CD81, we did not observe a
573 reduced entry efficiency of HCVpp. However, in vivo, the defect in CD81 binding seemed
574 to be dominant, likely due to lower receptor expression levels of hepatocytes.

575 Currently, it appears as a paradigm that virus genomes adapted to cell culture are impaired
576 in vivo. In fact, most available HCV full-length WT genomes are infectious in vivo, either
577 in chimpanzees or in human liver chimeric mice, but do not replicate in cell culture.
578 Unfortunately, limited information is available on the infectivity of their cell culture adapted
579 counterparts (26). Indeed, initial studies on gt1b Con1 revealed that particularly highly
580 adaptive mutations in NS5A attenuated the isolate in vivo and reverted to WT in
581 chimpanzees (19). A similar negative correlation and reversions to WT were found in case
582 of gt1a H77S.2, which initiated a chronic infection in a chimpanzee, but lost all 6 cell culture
583 adaptive mutations during the course of infection (47). Also for gt1a RTM, a negative
584 correlation between replication in vitro and in human liver chimeric mice was observed
585 (61). However, these phenotypes are not surprising, since all examples contain replication
586 enhancing mutations in NS5A. Since we now know that these mutations compensate for
587 PI4KA overexpression in Huh7 cells compared to hepatocytes (17), it is plausible, that they
588 are not beneficial to support replication in vivo. A number of comprehensive side-by-side
589 comparisons exists only for JFH-1-based constructs and here the picture is more diverse.
590 JFH-1 titer-enhancing mutations have been found to revert to WT upon infection of human
591 liver chimeric mice (21), suggesting again deleterious effects. However, JFH-1 WT had a
592 low capacity for virus production in cell culture and was less pathogenic than other WT
593 strains, requiring also further adaptation in chimpanzees (20, 62). In contrast, J6/JFH-1
594 chimeras generated much higher virus titers in vitro compared to JFH-1 and replicated more
595 robustly in vivo (41). Importantly, in case of J6/JFH-1, mutations in NS2 were identified
596 upon infection of human liver chimeric mice stimulating virus titers in vitro and in vivo
597 (63), thereby suggesting that both functions are not necessarily mutually exclusive. Also for
598 gt1b Con1, a replication enhancing mutation in NS4B was found to be compatible with
599 infectivity in vivo (18), therefore we chose it as a starting point for adaptation of GLT1.

600 This might be the reason why GLT1cc, albeit harboring 21 adaptive mutations, kept its
601 ability to replicate in vivo. Interestingly, while GLT1-20M behaved similar to H77S.2 in
602 human liver chimeric mice (47), by initiating only a low level, transient viremia, GLT1cc
603 was rescued by addition of only one critical titer-enhancing mutation (N2415S), replicating
604 as robustly as GLT1 WT in vivo, with a critical reversion only at one position in E2 (see
605 above). GLT1cc therefore represents the first highly cell culture adaptive isolate that has
606 retained its infectivity in vivo. By identification of a broader set of mutations facilitating
607 virus production in vivo and in vitro, as in case of N2415S, a more rationale based design
608 of additional infectious clones might become in reach.
609 Given the clinical significance and global abundance of gt1b infections, GLT1cc closes a
610 significant gap in the availability of HCV clones capable of undergoing the entire replication
611 cycle in cell culture and will represent an important new tool for future vaccine development
612 and studies on HCV pathogenesis. It is still a long way to regularly culture patient-derived
613 isolates, which would be helpful to understand virus dynamics and heterogeneity and
614 instrumental for vaccine development. However, a better understanding of the molecular
615 mechanisms limiting virion morphogenesis in cell culture will at least allow a more
616 straightforward establishment of infectious culture models based on cloned isolates.
617

618 **Materials and Methods**

619 Reagents

620 The specific PI4KA inhibitor PI4KA-G1 was provided by Glaxo-Smith-Kline (64); the
621 CKIa-specific inhibitor H479 has been described previously (65). The PCi treatment was
622 used in a final concentration of 0.1µM G1 and 5µM H479 (17). The HCV neutralizing anti-
623 E2 antibodies AP33 or Fab mix (AR3C-HC84.1 Fab mixture) (66) were used at a
624 concentration of 10 µg/ml. The mouse monoclonal antibody AP33 recognizes conserved

625 residues within the HCV E2 amino acid region 412 to 423 and efficiently neutralizes diverse
626 HCV genotypes in cultured cells (37, 38). The monoclonal IgG2α mouse antibody 9E10
627 was used for detection of NS5A by immunofluorescence (dilution 1:1,000). PI4P was
628 visualized using a monoclonal IgM mouse antibody (Z-P004; Echelon) with a dilution of
629 1:200. As secondary antibody for immunofluorescence, anti-mouse IgG/IgM AlexaFluor
630 488 and anti-mouse IgG/IgG2α AlexaFluor 546 (both Invitrogen) were used. To detect
631 SEC14L2 in western blot, a monoclonal rabbit antibody (Abcam) was used at a dilution of
632 1:5,000. As secondary antibody for western blot, a goat anti-rabbit HRP antibody (Sigma-
633 Aldrich) was used.
634
635 Plasmid constructs
636 To generate cell lines stably expressing SEC14L2 the previously described pWPI-BLR
637 SEC14L2 (isoform 1) construct was used (16).
638 For replication studies, pFK i341 PiLuc NS3-3′ Con1 WT, pFK i341 PiLuc NS3-3′ Con1
639 K1846T (mut4B), pFK i341 PiLuc NS3-3′ Con1 S2204R (mut5A), pFK i341 PiLuc NS3-
640 3′ Con1 R2884G (mut5B) (28) and pFK i341 PiLuc NS3-3′ JFH-1 WT (67) have been
641 described previously. pFK i341 PiLuc NS3-3′ GLT1 K1846T (mut4B), pFK i341 PiLuc
642 NS3-3′ GLT1 S2204R (mut5A), pFK i341 PiLuc NS3-3′ GLT1 R2884G (mut5B) were
643 generated with oligonucleotides as specified in Table S1. Subgenomic replicons of GLT1-
644 20M and GLT1cc were constructed with the NEBuilder HiFi DNA assembly cloning kit
645 (New England Biolabs) according to the manufacturer's instructions using oligonucleotides
646 as specified in Table S1.
647 For CLEM experiments, the pTM NS3-5B GLT1-NS5A_mCherry construct with an in-
648 frame insertion of mCherry in domain 3 of NS5A (placement according to previous

649 descriptions (68)) was generated. pTM vectors allow for transient protein expression of
650 HCV non-structural proteins under control of the T7 promotor.
651 For infection experiments, plasmids encoding full-length genomes of JC1 (24), Con1 WT
652 (11) and DBN3acc (36) have been described elsewhere. pFK GLT1-mut4B, pFK GLT1-
653 mut4B+N2415S, pFK GLT1-20M+N2415S (GLT1cc), pFK Con1/C3GLT1 and pFK
654 GLT1cc L437F were generated with oligonucleotides as specified in Table S1.
655 For studies on particle production, pFK i389 JCN2A and pFK i389 JCN2AΔGDD have
656 been described elsewhere (43). pFK i389 JCN2AΔE1E2, pFK i389 GLT1/C3JFH-1 N2A
657 and pFK i389 GLT1cc/C3JFH-1 N2A were created with oligonucleotides as specified in
658 Table S1.
659 Regarding the HCVpp, pCMVΔ8.74 (69), pHR'CMVLuc (35) and pcDNAΔcE1E2-Con1
660 (68) were described previously. To create the expression vectors for the HCVpp of GLT1
661 and GLT1cc, oligonucleotides were used as specified in Table S1.
662
663 Cell lines
664 All eukaryotic cells were cultured at 37 °C in a constant humid atmosphere containing 5%
665 (v/v) CO_2. Cells were cultured in plastic dishes or flasks in Dulbecco's modified Eagle's
666 medium (DMEM; Gibco) containing 10% (v/v) FCS (Seromed; inactivated for 30 min at
667 56 °C), 1% (v/v) penicillin/streptomycin (10,000 U ml^{-1} penicillin, 10,000 µg ml^{-1}
668 streptomycin; Gibco), 2 mM L-glutamine (Gibco) and 1% (v/v) 100× non-essential amino
669 acids (Gibco). The identity of all basic cell lines (Huh7 High Passage, Huh7-Lunet and
670 Huh7.5) was verified by a Multiplex human cell line authentication test. All cell lines were
671 regularly tested to check they were free of mycoplasma contamination using a commercially
672 available system (MycoAlert Mycoplasma Detection kit; Lonza). HCV replication
673 experiments were conducted using the highly permissive human hepatoma cell line Huh7

674 High Passage (28) or the sub-clones Huh7-Lunet (17) or Huh7.5 (29). Huh7-Lunet T7 stably
675 express the T7 RNA polymerase (70). Ectopic CD81 expression is required due to low
676 expression in Huh7-Lunet (35). Huh7-Lunet CD81N, selected for the absence of CD81,
677 have been described elsewhere (34). Huh7-Lunet CD81 cells stably expressing MAVS–
678 GFP–NLS (32) have been described (17). Expression of MAVS–GFP–NLS or MAVS-
679 mCherry-NLS allowed detection of HCV replication in individual live cells. The construct
680 encodes enhanced GFP or mCherry respectively with an NLS fused to the carboxy-terminus
681 of MAVS, containing an HCV NS3/4A cleavage site and tagging the protein to
682 mitochondria. Huh7-Lunet; Huh7 and Huh7.5 cells expressing SEC14L2 were generated
683 with lentiviral vectors based on plasmid pWPI-BLR SEC14L2 (isoform 1) (16), expression
684 was maintained by selection with blasticidin (5 µg/ml).
685
686 Patient information
687 Serum for isolation of GLT1 was obtained from a male patient under immunosuppression
688 with tacrolimus, mycophenolic acid and methylprednisolone because of status post re-liver-
689 transplantation. For chronic HCV-infection the patient had been treated with pegylated
690 interferon α/ribavirin 10 years before and with pegylated interferon α/ribavirin/sofosbuvir
691 1 year before. The local ethics committee approved data collection and analysis (ethics vote:
692 S-677/2020, Heidelberg University, ethics committee of the medical faculty).
693
694 RNA extraction
695 RNA was extracted from hepatoma cells using the NucleoSpin RNA plus kit (Macherey-
696 Nagel) according to the manufacturer's instructions.
697 GLT1 infected human liver chimeric mice were sacrificed at 8 weeks post infection. After
698 collection of the livers, 100 mg of tissue samples were preserved frozen in 1.5 ml RNAlater

699 solution (ThermoFisher Scientific). To extract RNA, 20 mg of tissue were grinded to
700 powder using a Dounce tissue grinder set (Merck) on dry ice. RNA was then isolated using
701 the Bio&SELL RNA-Mini Kit (Bio&SELL) according to the manufacturer's protocol.
702 RNA was extracted from the human GLT1 patient serum as well as from the serum of
703 GLT1-mut4B, -20M and GLT1cc infected human liver chimeric mice using the NucleoSpin
704 Virus kit (Macherey-Nagel) according to the manufacturer's instructions.
705
706 Sequence analysis of viral populations
707 GLT1 WT sequence was obtained from total RNA extracted from Huh7-Lunet CD81 cells
708 infected with Serum 1 and treated with PCi (17). cDNA synthesis and nested PCR
709 amplification of the HCV coding sequence and parts of the noncoding sequence was done
710 in three overlapping fragments with the Expand-RT and Expand-long-PCR system (Roche)
711 using primers and protocols as described for Con1 (Table S1, (11)). By direct sequencing
712 of PCR products a consensus sequence was obtained and synthesized (GeneCust Europe).
713 The termini of the genome (1-80 and 3' half of the x-tail) were taken from the Con1
714 sequence.
715 For analysis of the GLT1 cell culture adaptation as well as for the HCV population in
716 infected mice, isolated RNA was converted into cDNA using the SuperScript IV First-
717 Strand Synthesis kit (Invitrogen) with the HCV specific 3´NTR antisense primer A_9416
718 (Table S1) according to the manufacturer's instructions. From the cDNA, the HCV genome
719 was amplified in three overlapping fragments via nested PCR using the platinum SuperFi II
720 DNA polymerase kit (Invitrogen) with oligonucleotides as specified in Table S1. After the
721 nested PCR, PCR products were purified via agarose gel electrophoresis and directly
722 sequenced. In case of GLT1-20M, the consensus of the coding sequence was synthesized
723 (GeneArt) and inserted into the GLT1 WT construct.

724 In order to extract individual viral clones from the pooled PCR samples derived from the
725 cDNA, the TOPO XL-2 Complete PCR Cloning Kit (Invitrogen) was used according to the
726 manufacturer's instructions.
727
728 In vitro transcription of HCV RNA, electroporation of cells and luciferase activity assay
729 In vitro transcription, electroporation and luciferase assays were performed as described
730 elsewhere (28). In brief, 2.5-5 µg of in vitro transcribed viral RNA was electroporated into
731 2-4x10^6 cells for Huh7-Lunet or Huh7 High Passage cells, or 3-6x10^6 cells for Huh7.5 cells.
732 The cells were seeded into 6- or 12-well plates and treated with DMSO or PCi (5 µM H479
733 / 0.01 µM G1) (17) after four hours. Afterwards, the cells were harvested at the indicated
734 time points, and luciferase activity was determined in duplicates using a tube luminometer
735 (Lumat LB9507; Berthold Technologies). If applicable, luciferase activity at 4 h after
736 transfection was used for normalization to account for varying transfection efficiency. Nano
737 luciferase measurements were performed with the Nano-Glo Luciferase Assay System
738 (Promega) according to the manufacturer's instructions.
739
740 Low precision correlative-light-electron-microscopy (low-precision CLEM)
741 For the analysis of the replication organelles in the replication competent system, 4x10^4
742 electroporated Huh7-Lunet CD81 MAVS-GFP-NLS cells with or without SEC14L2
743 expression were seeded in a 6 cm dish with a grid on the bottom (MatTek Corporation) and
744 were incubated at 37 °C for 48 hours. In case of the expression model, 4x10^4 Huh7-Lunet
745 T7 cells with or without SEC14L2 expression were seeded in a 6 cm dish with a grid on the
746 bottom (MatTek Corporation) and were transfected 24 hours later with pTM NS3-5B GLT1
747 NS5A_mCherry. Prior to the fixation either the nuclear GFP localization or the
748 NS5A_mCherry signal was used to determine regions on the grid with a high number of

749 HCV positive cells. Afterwards, cells were fixed with with 2.5% GA, 2% sucrose in 50 mM
750 sodium cacodylate buffer (CaCo), supplemented with 50 mM KCl, 2.6 mM $MgCl_2$ and
751 2.6 mM $CaCl_2$ for at least 30 min on ice. After three washes with 50 mM CaCo, samples
752 were incubated with 2% osmium tetroxide in 25 mM CaCo for 40 min on ice, washed three
753 times with EM-grade water and incubated in 0.5% uranyl acetate in water overnight at 4°C.
754 Samples were rinsed three times with water, dehydrated in a graded ethanol series (from
755 40% to 100%) at RT, embedded in Epon 812 (Electron Microscopy Sciences) and
756 polymerized for at least 48 h at 60 °C. After polymerization, the negative imprint of the
757 coordinate system from the gridded coverslip was used to identify the areas of interest for
758 ultrathin sections of 70 nm by sectioning with an ultramicrotome Leica EM UC6 (Leica
759 Microsystems) and were afterwards mounted on a slot grid. Sections were counterstained
760 using 3% uranyl acetate in 70% methanol for 5 min and lead citrate (Reynold's) for 2 min
761 and imaged by using a JEOL JEM-1400 (JEOL) operating at 80 kV and equipped with a 4K
762 TemCam F416 (Tietz Video and Image Processing Systems).
763
764 Production of cell culture derived virus
765 Production of virus was performed as described elsewhere (18). Briefly, full-length RNA
766 genomes were electroporated into Huh7-Lunet or Huh7.5 cells. Supernatants were collected
767 at 24 and 48 hours after transfection and filtered through 0.45 µm filter units. Afterwards,
768 the collected supernatants of each isolate were concentrated using a Centricon Plus-70
769 centrifugal filter device (100 K nominal molecular weight limit; Millipore) resulting in an
770 approximately 100x concentrated stock (v/v) that was aliquoted and stored at -80 °C.
771
772 Core-ELISA

773 For the determination of extracellular core protein level, 900 µl supernatant was filtered
774 (0.45 µm filter) and 100 µl 10% Triton X100-PBS was added to a final concentration of 1%
775 Triton X100. Intracellular core protein was determined by resuspension of ~$1x10^6$ cells in
776 1 ml 1% Triton X100-PBS. Core protein was quantified using a commercial
777 chemiluminescent microparticle immunoassay (ARCHITECT HCV Ag Reagent kit; Abbot
778 Diagnostics) according to the manufacturer's instructions. Samples were analyzed by the
779 central laboratory for diagnostic at the University Hospital Heidelberg.
780
781 TCID50
782 To assess the tissue culture infectious dose (TCID50) of virus containing supernatant or
783 virus stock, we seeded Huh7-Lunet CD81 MAVS-GFP-NLS cells at a concentration of
784 $1x10^4$/well in a 96-well plate 24 hours prior to the infection. The medium was aspirated and
785 200 µl of a 1:10 diluted inoculum was added to the first row, followed by a subsequent 1:10
786 dilution in each row. After 4 hours, the inoculum was removed, fresh DMEM medium was
787 added to the cells and incubated for 72 hours at 37°C with 5% CO_2. Cells were washed once
788 with PBS and fixed with 4% PFA for 20 min at RT, followed by two wash steps with PBS.
789 The infection status of each individual well was determined by fluorescent microscopy
790 based on the location of the GFP signal. The TCID50 was calculated using the method of
791 Spearman and Kärber as described previously (71).
792
793 Real-time quantification PCR (Taqman qPCR)
794 HCV RNA copies were determined by Taqman RT-qPCR using a Quanta BioSciences
795 qScript XLT One- Step RT-qPCR kit according to the manufacture's instruction (Bio-Rad).
796 GLT1_probe was used to detect for GLT1 RNA, together with the S_59 & A_165 primers
797 (Table S1). For detection of JC1 RNA, JC1_probe was used together with the S_146 &

798 A_219 primers. Taqman RT-qPCRs were run in triplicate together with an HCV RNA
799 standard for each isolate of known quantity and analyzed using Bio-Rad CFX96 software.
800
801 Passaging of cells and supernatants
802 5 µg of in vitro transcribed viral full-length RNA was electroporated into $4x10^6$ Huh7-Lunet
803 CD81 cells either expressing SEC14L2 or not. The cells were seeded in a 6-well dish 1:1
804 together with non-electroporated cells expressing additionally a MAVS-GFP-NLS reporter
805 protein. After 72-96 hours, the cells were expanded/passaged in a 1:5 dilution. At the
806 indicated time points, the supernatant (~60 ml) of three 15 cm-diameter dishes was
807 concentrated (~600 µl) and used for infection of previously seeded (12-well) $4x10^4$ Huh7-
808 Lunet CD81 MAVS-GFP-NLS cells with or without SEC14L2 expression. 4 hours post
809 infection, the inoculum was removed, replaced with 1 ml fresh DMEM medium and
810 incubated for 72 hours at 37 °C with 5% CO_2. The putative infected cells were fixed with
811 4% PFA and manually analyzed for nuclear GFP signal. In case of GLT1-mut4B p29 and
812 all the following supernatant passages, the infected cells, instead of the initially
813 electroporated cells, were expanded/passaged each 72-96 hours as described above. After
814 the indicated passage number, supernatant (~7 ml) from a 10 cm-diameter-dish was used to
815 infect previously seeded (10 cm-diameter-dish) $1x10^5$ Huh7-Lunet CD81 MAVS-GFP-
816 NLS for 4 hours. Afterwards the inoculum was removed, replaced with 8 ml fresh DMEM
817 medium and incubated for 72-96 hours. Prior to each cell passaging and/or supernatant
818 transfer the number of nuclear GFP signals within the culture was estimated via
819 fluorescence microscopy.
820
821 Production and purification of recombinant Fab fragments

822 Fabs from antibodies HC84.1 and AR3C were cloned and produced as described previously
823 (66). Briefly, codon-optimized synthetic genes (Genscript) encoding heavy and light chains
824 of the Fab regions were cloned into a bicistronic Drosophila S2 Fab expression vector
825 comprising a double Strep tag at the C-terminus of the heavy chain and an N-terminal BiP-
826 signal sequence for efficient translocation of each chain. Next, stably transfected S2 cell
827 lines were induced with 4 μM $CdCl_2$ at a density of approximately $6x10^6$ cells/ml for Fab
828 production. After 6 days, Fabs were purified from the cell supernatant using affinity
829 chromatography (Strep Tactin XT Superflow resin, IBA) followed by size exclusion
830 chromatography (SEC; HiLoad 26/600 Superdex 200 pg column, GE Healthcare). Both
831 proteins were mixed in a molecular ratio 1:1 and the AR3C-HC84.1 Fab mixture was re-
832 purified by SEC on a Superdex 200 Increase 10/300 GL column (GE Healthcare) with PBS
833 as the eluent.
834
835 Viral spread assay
836 HCV positive Huh7-Lunet CD81 MAVS-GFP-NLS, either electroporated or passaged cells,
837 were co-seeded in a 12-well dish with naïve Huh7-Lunet CD81 MAVS-mCherry-NLS in a
838 ratio of 1:5. The cells were harvested at indicated time points with 4% PFA-PBS for 20 min
839 at RT. Each well was additionally stained with DAPI. Afterwards, the whole well was
840 imaged using a Celldiscoverer 7 microscope using an Axiocam 712 and a Plan-Apochromat
841 5x/0.35 objective (all Carl Zeiss Microscopy).
842
843 Quantification of nuclear GFP or mCherry in Huh7-Lunet CD81 cells
844 To segment nuclei in stitched images we trained a Random Forest classifier based on the
845 DAPI signal using iLastik (72) which predicts semantic class attribution (nucleus or
846 background) for every pixel. Objects obtained in this way were subsequently filtered by size

847 to exclude unusually small or large nuclei which often represent aberrant biological
848 structures or microscopy artefacts. Hysteresis algorithm was used to separate nuclei in close
849 proximity to each other. In the next step, using iLastik object classification workflow, a
850 machine learning algorithm was trained to classify objects into three categories – infected,
851 non-infected and HCV spreading "seed" cells based on the localization of the infection
852 reporters in GFP and mCherry channel. The training set of data was arbitrary selected, and
853 the same machine learning algorithm was used for the pixel and object classification in all
854 images.
855
856 Quantification of cell distribution and foci of infected cells
857 Based on the automated image analysis and cell classification by iLastik, the spatial
858 distribution of donor and recipient cells, as well as quantification of individual foci of
859 infected cells was evaluated as follows. Distances between two individual cells were
860 calculated based on the Eucledian distance, i.e., $d = \sqrt{(x_1 - x_2)^2 + (y_1 - y_2)^2}$ with (x_1,y_1)
861 and (x_2,y_2) defining the positions of the nuclei of the cells as identified by iLastik. As image
862 analysis does not allow visualization of contacts of individual cell membranes, we
863 determined the cell composition within the local surrounding of a donor cell by considering
864 all cells with nuclei positions within a certain radius r around the cell. With individual cells
865 assumed to have a diameter of 20-30 µm, we set r = 50 µm, but also tested other radii (30
866 µm, 100 µm) which did not change our results. Cellular composition was then assessed by
867 the cell type classifications of all cells within this area as obtained from iLastik.
868 Furthermore, we determined the minimal distance of each donor cell to the nearest recipient
869 cell by calculating the distances between each of the different cell types and sorting them
870 accordingly. Foci of infected cells were determined by considering each cell within a certain
871 distance d_n to be in contact to the other cell. Individual foci and their sizes were then

872 assessed by counting all connected donor and recipient cells. We defined donor foci as those
873 that contained at least one donor cell, and growing donor foci comprising at least one donor
874 and recipient cell each. As before, $d_n$was set to 50 µm to define connected cells, with the
875 use of other values (d_n = 30 µm) not changing our results.
876
877 HCVpp
878 Human Immunodeficiency virus (HIV)-based particles bearing HCV envelope proteins
879 were produced by HEK293T cells. $1.2x10^6$ cells were seeded in a 6 cm-diameter-dish and
880 transfected with 2.16 µg envelope protein expression construct pcDNAΔcE1E2-Con1 (68),
881 pcDNAΔcE1E2-GLT1 or pcDNAΔcE1E2-GLT1cc, 6.42 µg HIV gag-pol expression
882 construct pCMVΔ8.74 (69) and 6.42 µg firefly luciferase transducing retroviral vector (73)
883 using polyethylenimine (PEI). Medium was replaced after 6 h. After 48 h, supernatant
884 containing the pseudoparticles was passed through a 0.45 µm filter and used to infect $4x10^4$
885 naïve Huh7-Lunet CD81 cells seeded in a 12-well plate the day before. After 72 h, luciferase
886 assay was performed. SYBR Green based Product Enhanced Reverse Transcriptase assay
887 (SG-PERT) was performed using the Takyon SYBR green kit (Eurogentec) to quantify
888 HCVpp titers used for infection (74).
889
890 Sequence analysis
891 358 full-length HCV gt1b polyprotein sequences were obtained from the NIAID Virus
892 Pathogen Database and Analysis Resource (ViPR) (75) through the web site at
893 http://www.viprbrc.org/. With these sequences, a phylogenetic tree based on the minimum
894 evolution principle (76) was constructed and visualised with FigTree (v1.4.4). The gt1b
895 consensus sequence was generated with the HCV sequences used for the phylogenetic tree;
896 sequences were aligned with Clustal Omega and the consensus sequence was derived with

897 the EMBOSS Cons tool, both from the EMBL-EBI sequence analysis tools (77). The dataset
898 underlying the gt1b consensus was further used to determine the frequency of the mutations
899 arising in GLT1cc with the help of the Metadata-driven Comparative Analysis Tool (meta-
900 CATS) of ViPR (78).
901
902 Mice
903 Human liver chimeric mice were generated by transplantation of approximately 10^6 primary
904 human hepatocytes (donor L191501 from Lonza, Switzerland) into homozygous $uPA^{+/+}$-
905 SCID mice as previously described (79). Human albumin quantification in mouse plasma
906 was used to assess the level of liver humanization. Mice (n=3 per group) were infected by
907 intrasplenical injection of the respective viral inoculum (GLT1-1M, GLT1-20M and
908 GLT1cc). Blood plasma was collected at a two-weekly base and the plasma HCV load was
909 determined by RealStar® HCV RT-qPCR (Altona Diagnostics) following total nucleic acid
910 extraction (NucliSENS® EasyMag®, BioMérieux).
911
912 Software
913 Fluorescence, western blot and electron microscopy images were analyzed using Fiji.
914 Sequence alignments were visualized with AlignX, Sanger sequencing results were
915 analyzed and visualized with ContigExpress both of the Vector NTI software package (Life
916 Technologies). Analysis of the spatial distribution of cells was performed in R
917 (https://cran.r-project.org). Figures were arranged with Adobe Photoshop and Adobe
918 Illustrator. Schematics were created with BioRender.com.
919
920 Statistical analysis

921 Statistical analyses were performed using GraphPad Prism 8. Unless otherwise indicated,
922 statistics of data following a normal distribution and having similar variance were calculated
923 using an unpaired two-tailed Student's t-test.
924

925 **Acknowledgments**

926 We thank R. Klein, U. Herian and L. Verhoye for excellent technical assistance. We are
927 grateful for R. De Francesco for providing the CKIa innhibitor H479 and for Glaxo-
928 Smithkline for providing the PI4KA inhibitor G1. We thank T. von Hahn and S. Ciesek for
929 the pWPI-BLR SEC14L2 (isoform 1) construct, T. Wakita for the JFH-1 isolate, J. Bukh
930 for the DBN3acc isolate, D. Trono for retroviral expression constructs, I. Ambiel and O.
931 Fackler for SG-PERT RT standards and C. Rice for Huh7.5 cells and the 9E10 antibody.
932 We also thank the Infectious Disease Imaging Platform (IDIP) headed by V. Laketa for
933 facility use and help with microscopy. We are grateful to the Electron Microscopy Core
934 Facility (Heidelberg University) headed by S. Hillmer for providing access to their
935 equipment and for excellent support.
936

937 **Funding:** Deutsche Forschungsgemeinschaft: (DFG) LO1556/4-2 (278191845), TRR179
938 (272983813) and TRR209 (314905040) (to VoL and RBa), German Center for Infection
939 Research (DZIF) (TTU 05.821) (to VoL) and (TTU 05.712) (to RBa). AHP was funded by
940 the UK Medical Research Council grant MC_UU12014/2. LJS is funded by the Deutsche
941 Forschungsgemeinschaft - Projektnummer 158989968 - SFB 900, within project B10. FG
942 was supported by the Chica and Heinz-Schaller Foundation. PM was supported by an
943 Excellence of Science grant from the Research Foundation – Flanders (FWO) and FNRS;
944 and grants from the Ghent University Special Research Fund (UGent BOF).
945

946 **Author contributions:** Each author's contribution(s) to the paper should be listed (we
947 suggest following the CRediT model with each CRediT role given its own line. No
948 punctuation in the initials.

949 Conceptualization: VoL
950 Methodology: FG, ViL, CH, PaR
951 Software: FG, ViL
952 Investigation: CH, PaR, RBu, JYL, UH, PhR, OC, CST, NS
953 Visualization: LJS
954 Resources: PS, UM, RBa, AHP, TK, PM
955 Supervision: VoL, PM
956 Writing—original draft: CH, PaR, VoL
957 Writing—review & editing: VoL, PaR, CH, TK, RBa, PM, RBu, JYL, AHP, PhR,
958 NS, OC, CST, UM

959

960 **Competing interests:** Authors declare that they have no competing interests.

961

962 **Data and materials availability:** All data are available in the main text or the
963 supplementary materials. Sequences of GLT1 and GLT1cc are available under GenBank
964 accessions OM222702 and OM222703 respectively.

965

966 **References**

967 1. WHO. Global Hepatitis Report. 2017.
968 2. Poynard T, Yuen MF, Ratziu V, Lai CL. Viral hepatitis C. Lancet. 2003;362(9401):2095-
969 100.
970 3. Rockstroh JK, Ingiliz P, Petersen J, Peck-Radosavljevic M, Welzel TM, Van der Valk M,
971 et al. Daclatasvir plus sofosbuvir, with or without ribavirin, in real-world patients with HIV-HCV
972 coinfection and advanced liver disease. Antivir Ther. 2017;22(3):225-36.
973 4. WHO. Global Health Sector Strategy (GHSS) on viral hepatitis 2016–2021. 2016.

974 5. Bukh J, Miller RH, Purcell RH. Genetic heterogeneity of hepatitis C virus: quasispecies
975 and genotypes. Semin Liver Dis. 1995;15(1):41-63.
976 6. Simmonds P, Bukh J, Combet C, Deleage G, Enomoto N, Feinstone S, et al. Consensus
977 proposals for a unified system of nomenclature of hepatitis C virus genotypes. Hepatology.
978 2005;42(4):962-73.
979 7. Scheel TK, Simmonds P, Kapoor A. Surveying the global virome: identification and
980 characterization of HCV-related animal hepaciviruses. Antiviral Res. 2015;115:83-93.
981 8. Borgia SM, Hedskog C, Parhy B, Hyland RH, Stamm LM, Brainard DM, et al.
982 Identification of a Novel Hepatitis C Virus Genotype From Punjab, India: Expanding
983 Classification of Hepatitis C Virus Into 8 Genotypes. J Infect Dis. 2018;218(11):1722-9.
984 9. Daw MA, El-Bouzedi AA, Ahmed MO, Dau AA, Agnan MM, Drah AM. Geographic
985 integration of hepatitis C virus: A global threat. World J Virol. 2016;5(4):170-82.
986 10. Lohmann V. Hepatitis C virus RNA replication. Curr Top Microbiol Immunol.
987 2013;369:167-98.
988 11. Lohmann V, Korner F, Koch J, Herian U, Theilmann L, Bartenschlager R. Replication of
989 subgenomic hepatitis C virus RNAs in a hepatoma cell line. Science. 1999;285(5424):110-3.
990 12. Blight KJ, Kolykhalov AA, Rice CM. Efficient initiation of HCV RNA replication in cell
991 culture. Science. 2000;290:1972-4.
992 13. Lohmann V. Hepatitis C virus cell culture models: an encomium on basic research paving
993 the road to therapy development. Medical microbiology and immunology. 2019;208(1):3-24.
994 14. Kato T, Date T, Miyamoto M, Furusaka A, Tokushige K, Mizokami M, et al. Efficient
995 replication of the genotype 2a hepatitis C virus subgenomic replicon. Gastroenterology.
996 2003;125(6):1808-17.
997 15. Saeed M, Andreo U, Chung HY, Espiritu C, Branch AD, Silva JM, et al. SEC14L2
998 enables pan-genotype HCV replication in cell culture. Nature. 2015;524(7566):471-5.
999 16. Costa R, Todt D, Zapatero-Belinchon F, Schenk C, Anastasiou OE, Walker A, et al.
1000 SEC14L2, a lipid-binding protein, regulates HCV replication in culture with inter- and intra-
1001 genotype variations. J Hepatol. 2019;70(4):603-14.
1002 17. Harak C, Meyrath M, Romero-Brey I, Schenk C, Gondeau C, Schult P, et al. Tuning a
1003 cellular lipid kinase activity adapts hepatitis C virus to replication in cell culture. Nat Microbiol.
1004 2016;2:16247.
1005 18. Pietschmann T, Zayas M, Meuleman P, Long G, Appel N, Koutsoudakis G, et al.
1006 Production of infectious genotype 1b virus particles in cell culture and impairment by replication
1007 enhancing mutations. PLoS Pathog. 2009;5(6):e1000475.
1008 19. Bukh J, Pietschmann T, Lohmann V, Krieger N, Faulk K, Engle RE, et al. Mutations that
1009 permit efficient replication of hepatitis C virus RNA in Huh-7 cells prevent productive replication
1010 in chimpanzees. Proc Natl Acad Sci U S A. 2002;99(22):14416-21.
1011 20. Wakita T, Pietschmann T, Kato T, Date T, Miyamoto M, Zhao Z, et al. Production of
1012 infectious hepatitis C virus in tissue culture from a cloned viral genome. Nat Med.
1013 2005;11(7):791-6.
1014 21. Kaul A, Woerz I, Meuleman P, Leroux-Roels G, Bartenschlager R. Cell culture adaptation
1015 of hepatitis C virus and in vivo viability of an adapted variant. J Virol. 2007;81(23):13168-79.
1016 22. Yanagi M, Purcell RH, Emerson SU, Bukh J. Hepatitis C virus: an infectious molecular
1017 clone of a second major genotype (2a) and lack of viability of intertypic 1a and 2a chimeras.
1018 Virology. 1999;262(1):250-63.
1019 23. Lindenbach BD, Evans MJ, Syder AJ, Wolk B, Tellinghuisen TL, Liu CC, et al. Complete
1020 replication of hepatitis C virus in cell culture. Science. 2005;309(5734):623-6.
1021 24. Pietschmann T, Kaul A, Koutsoudakis G, Shavinskaya A, Kallis S, Steinmann E, et al.
1022 Construction and characterization of infectious intragenotypic and intergenotypic hepatitis C virus
1023 chimeras. Proc Natl Acad Sci U S A. 2006;103(19):7408-13.

1024 25. Yi M, Villanueva RA, Thomas DL, Wakita T, Lemon SM. Production of infectious
1025 genotype 1a hepatitis C virus (Hutchinson strain) in cultured human hepatoma cells. Proc Natl
1026 Acad Sci U S A. 2006;103(7):2310-5.
1027 26. Ramirez S, Bukh J. Current status and future development of infectious cell-culture
1028 models for the major genotypes of hepatitis C virus: Essential tools in testing of antivirals and
1029 emerging vaccine strategies. Antiviral Res. 2018;158:264-87.
1030 27. Lohmann V, Körner F, Dobierzewska A, Bartenschlager R. Mutations in hepatitis C virus
1031 RNAs conferring cell culture adaptation. Journal Of Virology. 2001;75:1437-49.
1032 28. Lohmann V, Hoffmann S, Herian U, Penin F, Bartenschlager R. Viral and cellular
1033 determinants of hepatitis C virus RNA replication in cell culture. J Virol. 2003;77(5):3007-19.
1034 29. Blight KJ, McKeating JA, Rice CM. Highly permissive cell lines for subgenomic and
1035 genomic hepatitis C virus RNA replication. J Virol. 2002;76(24):13001-14.
1036 30. Romero-Brey I, Merz A, Chiramel A, Lee JY, Chlanda P, Haselman U, et al. Three-
1037 dimensional architecture and biogenesis of membrane structures associated with hepatitis C virus
1038 replication. PLoS Pathog. 2012;8(12):e1003056.
1039 31. Reiss S, Rebhan I, Backes P, Romero-Brey I, Erfle H, Matula P, et al. Recruitment and
1040 activation of a lipid kinase by hepatitis C virus NS5A is essential for integrity of the membranous
1041 replication compartment. Cell Host Microbe. 2011;9(1):32-45.
1042 32. Jones CT, Catanese MT, Law LM, Khetani SR, Syder AJ, Ploss A, et al. Real-time
1043 imaging of hepatitis C virus infection using a fluorescent cell-based reporter system. Nat
1044 Biotechnol. 2010;28(2):167-71.
1045 33. Timpe JM, Stamataki Z, Jennings A, Hu K, Farquhar MJ, Harris HJ, et al. Hepatitis C
1046 virus cell-cell transmission in hepatoma cells in the presence of neutralizing antibodies.
1047 Hepatology. 2008;47(1):17-24.
1048 34. Witteveldt J, Evans MJ, Bitzegeio J, Koutsoudakis G, Owsianka AM, Angus AG, et al.
1049 CD81 is dispensable for hepatitis C virus cell-to-cell transmission in hepatoma cells. J Gen Virol.
1050 2009;90(Pt 1):48-58.
1051 35. Koutsoudakis G, Herrmann E, Kallis S, Bartenschlager R, Pietschmann T. The level of
1052 CD81 cell surface expression is a key determinant for productive entry of hepatitis C virus into
1053 host cells. J Virol. 2007;81(2):588-98.
1054 36. Ramirez S, Mikkelsen LS, Gottwein JM, Bukh J. Robust HCV Genotype 3a Infectious
1055 Cell Culture System Permits Identification of Escape Variants With Resistance to Sofosbuvir.
1056 Gastroenterology. 2016;151(5):973-85.e2.
1057 37. Clayton RF, Owsianka A, Aitken J, Graham S, Bhella D, Patel AH. Analysis of
1058 Antigenicity and Topology of E2 Glycoprotein Present on Recombinant Hepatitis C Virus-Like
1059 Particles. 2002;76(15):7672-82.
1060 38. Owsianka A, Tarr AW, Juttla VS, Lavillette D, Bartosch B, Cosset F-L, et al. Monoclonal
1061 Antibody AP33 Defines a Broadly Neutralizing Epitope on the Hepatitis C Virus E2 Envelope
1062 Glycoprotein. 2005;79(17):11095-104.
1063 39. Law M, Maruyama T, Lewis J, Giang E, Tarr AW, Stamataki Z, et al. Broadly
1064 neutralizing antibodies protect against hepatitis C virus quasispecies challenge. Nature Medicine.
1065 2008;14(1):25-7.
1066 40. Keck ZY, Xia J, Wang Y, Wang W, Krey T, Prentoe J, et al. Human monoclonal
1067 antibodies to a novel cluster of conformational epitopes on HCV E2 with resistance to
1068 neutralization escape in a genotype 2a isolate. PLoS Pathog. 2012;8(4):e1002653.
1069 41. Lindenbach BD, Meuleman P, Ploss A, Vanwolleghem T, Syder AJ, McKeating JA, et al.
1070 Cell culture-grown hepatitis C virus is infectious in vivo and can be recultured in vitro. Proc Natl
1071 Acad Sci U S A. 2006;103(10):3805-9.
1072 42. Bartosch B, Dubuisson J, Cosset FL. Infectious hepatitis C virus pseudo-particles
1073 containing functional E1-E2 envelope protein complexes. J Exp Med. 2003;197(5):633-42.

1074 43. Schult P, Roth H, Adams RL, Mas C, Imbert L, Orlik C, et al. microRNA-122 amplifies
1075 hepatitis C virus translation by shaping the structure of the internal ribosomal entry site. Nature
1076 Communications. 2018;9(1):2613.
1077 44. Lindenbach BD. Virion assembly and release. Curr Top Microbiol Immunol.
1078 2013;369:199-218.
1079 45. Gottwein JM, Scheel TK, Jensen TB, Lademann JB, Prentoe JC, Knudsen ML, et al.
1080 Development and characterization of hepatitis C virus genotype 1-7 cell culture systems: role of
1081 CD81 and scavenger receptor class B type I and effect of antiviral drugs. Hepatology.
1082 2009;49(2):364-77.
1083 46. Burm R, Collignon L, Mesalam AA, Meuleman P. Animal Models to Study Hepatitis C
1084 Virus Infection. 2018;9.
1085 47. Yi M, Hu F, Joyce M, Saxena V, Welsch C, Chavez D, et al. Evolution of a cell culture-
1086 derived genotype 1a hepatitis C virus (H77S.2) during persistent infection with chronic hepatitis
1087 in a chimpanzee. J Virol. 2014;88(7):3678-94.
1088 48. Li YP, Ramirez S, Jensen SB, Purcell RH, Gottwein JM, Bukh J. Highly efficient full-
1089 length hepatitis C virus genotype 1 (strain TN) infectious culture system. Proc Natl Acad Sci U S
1090 A. 2012;109(48):19757-62.
1091 49. Date T, Kato T, Kato J, Takahashi H, Morikawa K, Akazawa D, et al. Novel cell culture-
1092 adapted genotype 2a hepatitis C virus infectious clone. J Virol. 2012;86(19):10805-20.
1093 50. Koutsoudakis G, Perez-del-Pulgar S, Coto-Llerena M, Gonzalez P, Dragun J, Mensa L, et
1094 al. Cell Culture Replication of a Genotype 1b Hepatitis C Virus Isolate Cloned from a Patient
1095 Who Underwent Liver Transplantation. PloS one. 2011;6(8):e23587.
1096 51. Date T, Morikawa K, Tanaka Y, Tanaka-Kaneko K, Sata T, Mizokami M, et al.
1097 Replication and infectivity of a novel genotype 1b hepatitis C virus clone. Microbiology and
1098 immunology. 2012;56(5):308-17.
1099 52. Murayama A, Date T, Morikawa K, Akazawa D, Miyamoto M, Kaga M, et al. The NS3
1100 helicase and NS5B-to-3'X regions are important for efficient hepatitis C virus strain JFH-1
1101 replication in Huh7 cells. J Virol. 2007;81(15):8030-40.
1102 53. Brimacombe CL, Grove J, Meredith LW, Hu K, Syder AJ, Flores MV, et al. Neutralizing
1103 antibody-resistant hepatitis C virus cell-to-cell transmission. J Virol. 2011;85(1):596-605.
1104 54. Yin C, Goonawardane N, Stewart H, Harris M. A role for domain I of the hepatitis C virus
1105 NS5A protein in virus assembly. PLoS Pathog. 2018;14(1):e1006834.
1106 55. Masaki T, Suzuki R, Murakami K, Aizaki H, Ishii K, Murayama A, et al. Interaction of
1107 hepatitis C virus nonstructural protein 5A with core protein is critical for the production of
1108 infectious virus particles. J Virol. 2008;82(16):7964-76.
1109 56. Appel N, Zayas M, Miller S, Krijnse-Locker J, Schaller T, Friebe P, et al. Essential role of
1110 domain III of nonstructural protein 5A for hepatitis C virus infectious particle assembly. PLoS
1111 Pathog. 2008;4(3):e1000035.
1112 57. Tellinghuisen TL, Foss KL, Treadaway J. Regulation of hepatitis C virion production via
1113 phosphorylation of the NS5A protein. PLoS Pathog. 2008;4(3):e1000032.
1114 58. Jirasko V, Montserret R, Lee JY, Gouttenoire J, Moradpour D, Penin F, et al. Structural
1115 and functional studies of nonstructural protein 2 of the hepatitis C virus reveal its key role as
1116 organizer of virion assembly. PLoS Pathog. 2010;6(12):e1001233.
1117 59. Ströh LJ, Nagarathinam K, Krey T. Conformational Flexibility in the CD81-Binding Site
1118 of the Hepatitis C Virus Glycoprotein E2. 2018;9.
1119 60. Drummer HE, Boo I, Maerz AL, Poumbourios P. A Conserved Gly⁴³⁶-Trp-
1120 Leu-Ala-Gly-Leu-Phe-Tyr Motif in Hepatitis C Virus Glycoprotein E2 Is a Determinant of CD81
1121 Binding and Viral Entry. 2006;80(16):7844-53.

1122 61. Arai M, Tokunaga Y, Takagi A, Tobita Y, Hirata Y, Ishida Y, et al. Isolation and
1123 Characterization of Highly Replicable Hepatitis C Virus Genotype 1a Strain HCV-RMT. PloS
1124 one. 2013;8(12):e82527.
1125 62. Kato T, Choi Y, Elmowalid G, Sapp RK, Barth H, Furusaka A, et al. Hepatitis C virus
1126 JFH-1 strain infection in chimpanzees is associated with low pathogenicity and emergence of an
1127 adaptive mutation. 2008;48(3):732-40.
1128 63. Prentoe J, Verhoye L, Velázquez Moctezuma R, Buysschaert C, Farhoudi A, Wang R, et
1129 al. HVR1-mediated antibody evasion of highly infectious in vivo adapted HCV in humanised
1130 mice. Gut. 2016;65(12):1988.
1131 64. Bojjireddy N, Botyanszki J, Hammond G, Creech D, Peterson R, Kemp DC, et al.
1132 Pharmacological and genetic targeting of the PI4KA enzyme reveals its important role in
1133 maintaining plasma membrane phosphatidylinositol 4-phosphate and phosphatidylinositol 4,5-
1134 bisphosphate levels. J Biol Chem. 2014;289(9):6120-32.
1135 65. Neddermann P, Quintavalle M, Di Pietro C, Clementi A, Cerretani M, Altamura S, et al.
1136 Reduction of hepatitis C virus NS5A hyperphosphorylation by selective inhibition of cellular
1137 kinases activates viral RNA replication in cell culture. J Virol. 2004;78(23):13306-14.
1138 66. Krey T, Meola A, Keck Z-y, Damier-Piolle L, Foung SKH, Rey FA. Structural Basis of
1139 HCV Neutralization by Human Monoclonal Antibodies Resistant to Viral Neutralization Escape.
1140 PLOS Pathogens. 2013;9(5):e1003364.
1141 67. Binder M, Quinkert D, Bochkarova O, Klein R, Kezmic N, Bartenschlager R, et al.
1142 Identification of determinants involved in initiation of hepatitis C virus RNA synthesis by using
1143 intergenotypic replicase chimeras. J Virol. 2007;81(10):5270-83.
1144 68. Schaller T, Appel N, Koutsoudakis G, Kallis S, Lohmann V, Pietschmann T, et al.
1145 Analysis of hepatitis C virus superinfection exclusion by using novel fluorochrome gene-tagged
1146 viral genomes. J Virol. 2007;81(9):4591-603.
1147 69. Dull T, Zufferey R, Kelly M, Mandel RJ, Nguyen M, Trono D, et al. A third-generation
1148 lentivirus vector with a conditional packaging system. J Virol. 1998;72(11):8463-71.
1149 70. Backes P, Quinkert D, Reiss S, Binder M, Zayas M, Rescher U, et al. Role of annexin A2
1150 in the production of infectious hepatitis C virus particles. J Virol. 2010;84(11):5775-89.
1151 71. Vieyres G, Pietschmann T. Entry and replication of recombinant hepatitis C viruses in cell
1152 culture. Methods. 2013;59(2):233-48.
1153 72. Berg S, Kutra D, Kroeger T, Straehle CN, Kausler BX, Haubold C, et al. ilastik:
1154 interactive machine learning for (bio)image analysis. Nat Methods. 2019;16(12):1226-32.
1155 73. Koutsoudakis G, Kaul A, Steinmann E, Kallis S, Lohmann V, Pietschmann T, et al.
1156 Characterization of the early steps of hepatitis C virus infection by using luciferase reporter
1157 viruses. J Virol. 2006;80(11):5308-20.
1158 74. Vermeire J, Naessens E, Vanderstraeten H, Landi A, Iannucci V, Van Nuffel A, et al.
1159 Quantification of reverse transcriptase activity by real-time PCR as a fast and accurate method for
1160 titration of HIV, lenti- and retroviral vectors. PloS one. 2012;7(12):e50859.
1161 75. Pickett BE, Sadat EL, Zhang Y, Noronha JM, Squires RB, Hunt V, et al. ViPR: an open
1162 bioinformatics database and analysis resource for virology research. Nucleic Acids Res.
1163 2012;40(Database issue):D593-8.
1164 76. Desper R, Gascuel O. Fast and accurate phylogeny reconstruction algorithms based on the
1165 minimum-evolution principle. J Comput Biol. 2002;9(5):687-705.
1166 77. Madeira F, Park YM, Lee J, Buso N, Gur T, Madhusoodanan N, et al. The EMBL-EBI
1167 search and sequence analysis tools APIs in 2019. Nucleic Acids Res. 2019;47(W1):W636-W41.
1168 78. Pickett BE, Liu M, Sadat EL, Squires RB, Noronha JM, He S, et al. Metadata-driven
1169 comparative analysis tool for sequences (meta-CATS): an automated process for identifying
1170 significant sequence variations that correlate with virus attributes. Virology. 2013;447(1-2):45-51.

1171 79. Meuleman P, Libbrecht L, De Vos R, de Hemptinne B, Gevaert K, Vandekerckhove J, et
1172 al. Morphological and biochemical characterization of a human liver in a uPA-SCID mouse
1173 chimera. Hepatology. 2005;41(4):847-56.
1174

1175 **Figures Legends**

1176 **Fig. 1: Phylogeny and RNA replication efficiency of GLT1 in Huh7-Lunet cells compared to**
1177 **other HCV isolates.** (**A**) Alignment of the GLT1 amino acid sequence compared to a gt1b
1178 consensus (upper part) or Con1 (lower part). Black lines indicate differences. (**B**) Phylogenetic tree
1179 of gt1b isolates available in ViPR (75). Some selected viral variants available and characterized as
1180 molecular clones are highlighted (GenBank accession numbers: HCV-N: AAB27127, HCV-AH1:
1181 BAG31965, HCV-NC1: BAM29294, HCV-O: BAD91386, Con1: CAB46677, HCV-J4:
1182 BAA01583; HCV-BK: AAA72945). (**C-F**) Replication efficiency of GLT1 compared to Con1 and
1183 JFH-1, using different replication enhancing conditions. Huh7-Lunet cells were transfected with
1184 subgenomic reporter replicons of the indicated isolates or mutants. Luciferase activity in cell lysates
1185 (RLU) was quantified as a correlate of RNA replication efficiency at the given time points and
1186 normalized to 4 h. Cells were either stimulated by PCi treatment (C,E) and/or SEC14L2 expression
1187 (D,E) compared to DMSO treatment or empty vector transduction, respectively. (**F**) Replication
1188 enhancement of GLT1 (green lines) or Con1 (black lines) by mutations in NS4B (K1846T), NS5A
1189 (S2204R) or NS5B (R2884G). (C-F) A replication deficient Con1 variant (Con1ΔGDD) was used
1190 as a negative control for replication and the respective luciferase level at 72 h is indicated by a
1191 dashed grey line in all diagrams and shown in a time-course in the Con1 panels. The data are the
1192 mean values from two independent experiments shown as individual data points with two technical
1193 replicates each.

1194

1195 **Fig. 2: Ultrastructural analysis of membrane rearrangements induced by the GLT1 replicon**
1196 **using correlative light and electron microscopy (CLEM).** Huh7-Lunet CD81 MAVS-GFP-NLS
1197 cells were transfected with GLT1 wildtype reporter replicons (GLT1rep) (WT) or a mutant
1198 encoding a replication enhancing mutation in NS4B (mut4B, K1846T). In case of GLT1rep WT
1199 replication was enhanced either by SEC14L2 expression or PCi treatment. The cells were fixed 48

1200 hours post electroporation and the nuclear GFP signal was used to identify positive cells for further
1201 analysis. DMV profiles were analyzed using TEM images taken at x4k magnification. For
1202 systematic random sampling, ~100 μm^2 rectangle areas were placed on a whole cell image and
1203 DMVs were counted. At least 6 positive cells were counted in each sample. (**A**) The number of
1204 DMVs per μm^2. (**B**) The diameter of DMVs. (**C**) Representative images of each condition.
1205

1206 **Fig. 3: Evaluation of virus production and passaging of GLT1.** (**A**) Detection of intra- and
1207 extracellular core protein after transfection of full-length virus genomes. Huh7-Lunet with or
1208 without SEC14L2 expression and/or with PCi treatment were transfected with the indicated HCV
1209 full-length genomes. 72 hours post transfection, the concentration of core protein in lysate
1210 (intracellular, light grey) and supernatant (extracellular, dark grey) of one well of a 6-well dish was
1211 quantified by ELISA, as correlates of RNA replication and virus production, respectively. Shown
1212 are data from two independent experiments. The dashed grey line indicates the detection limit of
1213 3 fmol/l core protein; n.d. = not detectable. Successful infection upon transfer of supernatants to
1214 naïve cells is shown on top of each condition. (**B**) Example of infection events upon supernatant
1215 transfer to MAVS-GFP-NLS cells. Infection is identified by nuclear GFP signal. (**C**) Huh7-Lunet
1216 CD81 cells with or without SEC14L2 expression were transfected with Con1 (blue) or GLT1 WT
1217 (green) or GLT1-mut4B (red) RNA and passaged. Before each passage, the amount of extracellular
1218 viral core protein was determined by ELISA. The dashed grey line represents the detection limit of
1219 3 fmol/l core protein. Arrows indicate timepoints of infections experiments with concentrated
1220 supernatant using Huh7-Lunet CD81 MAVS-GFP-NLS with or without SEC14L2 expression. (**D**)
1221 Infection events after transfer of concentrated supernatant following p29. (**E**) Extracellular amount
1222 of viral core protein over the course of additional rounds of supernatant transfer and cell passaging
1223 for GLT-mut4B in Huh7-Lunet CD81 MAVS-GFP-NLS cells. Each transfer event is indicated by
1224 the dashed grey lines, numbers below refer to the following cell passages. Three time points were

1225 highlighted with their total number of cell passages followed by the total number of supernatant
1226 passages (e.g. p118.27). Infections were either done with concentrated or pure supernatant as
1227 indicated on top. Grey triangles represent the approximate number of cells with a nuclear MAVS-
1228 GFP signal, shown in percent. (**F**) Consensus sequences derived by direct sequencing of RT-PCR
1229 products after p32.1 (first successful concentrated supernatant transfer), p64.8 (first pure
1230 supernatant transfer) and p118.27 (endpoint). Note that none of the changes reverted back to WT
1231 during passaging and were combined in a new synthetic genome termed GLT1-20M. (**G**)
1232 Determination of viral titers (TCID50/ml) from pure supernatant after either transfection of the
1233 indicated HCV full-length RNA or after the indicated passages of GLT1-mut4B. Shown are mean
1234 values and standard deviation of at least two independent experiments.
1235
1236 **Fig. 4: Characterization of cell-free and cell-to-cell spreading properties.** (**A**) Schematic
1237 representation of the experimental procedure to analyze viral spread. Below are representative
1238 pictures of the individual fluorescent microscopy channels, a merge file of all fluorescent channels
1239 as well as an image representing the classification after the analysis using different colors (far right).
1240 Nuclei shown with a yellow color (see #1) represent cells with a nuclear GFP signal classified as
1241 "donor" cells (nuclear GFP). Purple nuclei represent "recipient" cells after virus transmission in co-
1242 culture (nuclear mCherry). Orange nuclei represent "non-infected" cells (cytoplasmic
1243 mCherry/GFP, nuclear DAPI). (**B, C**) Huh7-Lunet CD81 MAVS-GFP-NLS cells transfected with
1244 full length HCV GLT1-mut4B, -20M or JC1 or obtained upon passaging of GLT-mut4B (Fig. 3E)
1245 were co-seeded with Huh7-Lunet MAVS-mCherry-NLS either (B) expressing CD81 or (C) a Huh7-
1246 Lunet variant sorted for low CD81 expression (34) in a ratio of 1:5 and incubated for 24-72 h. At
1247 the indicated time points, cells were fixed and the number of cells with a nuclear mCherry signal
1248 was determined via fluorescence microscopy followed by machine learning object classification.
1249 Black dots represent measurements for two independent experiments with the black line indicating

1250 the approximated mean time course. (**D**) Determination of the viral titer (TCID50/ml) from
1251 concentrated supernatant of different HCV isolates. The viral stocks were incubated with 10 µg/ml
1252 of anti-E2 broadly neutralizing antibodies, using either AP33 or Fab mix or mock treated for 1 h at
1253 37 °C prior to the infection of Huh7-Lunet CD81 MAVS-GFP-NLS. Shown are the mean and
1254 standard deviation of two independent experiments (black dots). (**E**) HCV positive Huh7-Lunet
1255 CD81 MAVS-GFP-NLS were co-seeded with Huh7-Lunet CD81 MAVS-GFP-NLS and analyzed
1256 after 72 h as in (B, C) but in presence of 10 µg/ml of either AP33 or Fab mix. Shown are the mean
1257 and standard deviation of two independent experiments (black dots). (**F**) Fraction of differently
1258 classified cell types within an area of 50 µm around a donor cell of GLT1-20M or JC1 treated with
1259 10 µg/ml of anti-E2 broadly neutralizing antibodies, either AP33 or Fab mix, 72 hours after seeding.
1260 (**G**) Frequency of individual donor (nuclear GFP) foci associated with at least one recipient (nuclear
1261 mCherry) cell within an area of 50 µm. This number shall represent an approximation of the
1262 likelihood of an individual donor cell infecting a non-infected cell in its surrounding.
1263

1264 **Fig. 5: Impact of N2415S on virion production of GLT1.** Huh7-Lunet CD81 MAVS-GFP-NLS
1265 were transfected with the indicated HCV genome variants, supernatants harvested at 24 and 48 h
1266 after transfection and concentrated 100-fold to determine (**A**) TCID50 on Huh7-Lunet CD81
1267 MAVS-GFP-NLS cells, (**B**) core protein secretion by ELISA, (**C**) viral RNA using RT-qPCR and
1268 (**D**) the number of infected Huh7-Lunet CD81 MAVS-GFP-NLS 72 h after infection with 100 µl
1269 virus stock by classification with 2 color iLastik (infected / non-infected) based on GFP
1270 localization. Colors of data points represent one independent biological repetition across each sub-
1271 panel.

1272

1273 **Fig. 6: Mechanisms of GLT1cc adaptation**. (**A**) Differences in amino acid sequence between
1274 GLT1 and GLT1cc and their abundance in other gt1b isolates are highlighted. Analysis based on
1275 358 full-length HCV gt1b polyprotein sequences derived from ViPR. Asterisk indicates adaptive
1276 mutation in NS4B of GLT1-mut4B. (**B**) Huh7-Lunet cells were transfected with subgenomic
1277 reporter replicons of the indicated isolates. Luciferase activity in cell lysates (RLU) was quantified
1278 as a correlate of RNA replication efficiency at the given time points and normalized to 4 h. The
1279 data are the mean values from three independent experiments shown as individual data points with
1280 two technical replicates each. (**C**) HCVpp bearing HCV envelope proteins of the indicated isolates
1281 on their surface were added to Huh7-Lunet CD81 cells. After 72 h, cells were lysed, and infectivity
1282 was determined based on a luciferase reporter in the HCVpp. Measurements were first normalized
1283 to the input determined via SG-PERT and then normalized to the resulting mean value of three
1284 replicates of the well-established Con1 isolate. Particles without envelope proteins (No env.) served
1285 as negative control. The data are the mean values from three independent experiments shown as
1286 individual data points with two technical replicates each. (**D**) Huh7-Lunet CD81 cells were
1287 transfected with the chimeric full-length HCV reporter construct depicted in the upper panel. It
1288 combines the sequence of the isolate of interest up to the C3 junction site in NS2 with the remaining
1289 part of the JFH-1 isolate (24). Therefore, the two mutations in NS2 contained in GLT1cc were not
1290 included in the chimeric genomes. RNA replication was determined at 72 hours post transfection
1291 (h.p.t.) and the supernatant was used to infect naïve Huh7-Lunet CD81 cells. At 72 hours post
1292 infection (h.p.i.), cells were lysed, and infectivity was determined via luciferase measurement. A
1293 replication deficient JC1 variant (JC1ΔGDD) and a JC1 variant lacking envelope proteins
1294 (JC1ΔE1E2) were used as negative controls for replication and infection respectively. The data are
1295 the mean values from two independent experiments shown as individual data points with two
1296 technical replicates each.

1297

1298 **Fig. 7: Infection of human liver chimeric mice**. (**A,C**) Human liver chimeric mice (n=3) were
1299 infected by intrasplenical injection of 50 µl pure high-titer post-transplant serum (A) or they were
1300 infected with concentrated supernatants obtained by transfection of GLT1-mut4B, GLT1-20M and
1301 GLT1cc (Fig. 5) (C). The plasma HCV load was determined at the designated time points using
1302 Realstar HCV RT-qPCR (Altona Diagnostics) following total nucleic acid extraction (NucliSENS,
1303 EasyMag). X = mouse found dead, n.d. = not detectable, LOD = limit of detection. (**B,D**) Consensus
1304 amino acid sequences were derived from mouse liver 8 weeks post-infection (B) or from mouse
1305 serum after 12 weeks (D, upper panel) or 6 weeks (D, lower panel) and subsequently compared to
1306 the respective input consensus sequences. (**E**) Viral titer (TCID50/ml) from concentrated
1307 supernatant of indicated HCV isolates harvested from Huh7-Lunet CD81 cells; data from two
1308 independent biological replicates.

1309

1310 **Fig. 8: Localization of the GLT1cc mutations within E2 and non-structural proteins.** The
1311 GLT1cc mutations are shown in sticks and highlighted in red. (**A**) Structure of the E2 core (grey)
1312 complexed with taumarin CD81 LEL (tCD81 LEL, sand) (PDB: 7MWX). Important E2 antibody
1313 binding epitopes named Epitope II and the CD81-binding loop are colored in green and deep purple,
1314 respectively. In the crystal structure a histidine is found at position 434 which was mutated *in silico*
1315 into a glutamine with the most abundant side chain conformation for clarity. (**B**) Model of NS2
1316 transmembrane segments (TMSs) according to TMS1 (PDB: 2JY0), TMS2 (PDB: 2KWT) and
1317 TMS3 (PDB: 2KWZ) are shown as separated entities in cartoon representation. They are tentatively
1318 placed into the schematically drawn membrane and the limits of transmembrane helices are given.
1319 (**C**) Structure of the NS3/4A N-terminal protease (PDB: 1A1R). Residues of the catalytic triad are
1320 shown in sticks and are colored in teal. For clarity, the isoleucine at position 1074 in the crystal
1321 structure was mutated *in silico* into a valine with the most abundant side chain conformation. (**D**)

1322 NS3 helicase is shown in complex with ssDNA (light pink) and the ATP mimic ADP·AIF4- (black,
1323 sticks) (PDB: 3kql). (**E**) The crystal structure of the NS5A Domain 1 from gt1b (PDB: 1ZH1) with
1324 the modelled N-terminal amphipathic helix (residues 1–33, PDB 1R7G) and the postulated RNA-
1325 binding groove between two monomers. (**F**) NS5B structure (PDB: 2D3U) featuring the
1326 characteristic fingers, palm, and thumb domains in light green, yellow and grey, respectively. The
1327 aspartic acid residues of the active site are shown in blue sticks for orientation.
1328

1329 **Supplementary Figure Legends**
1330
1331 **Fig. S1: SEC14L2 expression, schematic of the experimental procedure and replication**
1332 **efficiency of GLT1 in Huh7-Lunet cells.** (**A**) SEC14L2 expression levels in Huh7-Lunet, Huh7.5
1333 and Huh7 cells after lentiviral transduction with a SEC14L2 encoding vector or empty control,
1334 compared to PHH. Approximately $1x10^5$ Huh7-Lunet, Huh7.5, Huh7 or primary human
1335 hepatocytes (PHH) were lysed and analyzed by 10% SDS-PAGE/Western blotting for SEC14L2
1336 and Calnexin expression. One representative experiment from two independent repetitions is
1337 shown. (**B**) Schematic of a subgenomic reporter replicon and of the experimental procedure of
1338 luciferase-based replication measurement. HCV 5'UTR (HCV) poliovirus internal ribosomal entry
1339 site (IRES) (PV) and EMCV-IRES (EMCV), as well as the HCV 3'UTR are indicated by their
1340 respective secondary structures. NS3-NS5B and firefly luciferase coding regions are indicated by
1341 orange and yellow boxes, respectively. Transfection by electroporation is visualized by a lightning-
1342 symbol. (**C**) Replication enhancement by a combination of mutations and SEC14L2 expression for
1343 Con1 (left) and GLT1 (right). Huh7-Lunet cells either expressing SEC14L2 or transduced with
1344 empty vector were electroporated with the indicated subgenomic reporter replicon RNA containing
1345 mutations in NS4B (K1846T), NS5A (S2204R) or NS5B (R2884G) as indicated. Luciferase activity
1346 in cell lysates (RLU) was quantified as a correlate of RNA replication efficiency at the given time
1347 points and normalized to 4 h. A replication deficient Con1 variant (Con1ΔGDD) was used as a
1348 negative control and the respective luciferase level at 72 h is indicated by a dashed grey line in all
1349 diagrams. The data are the mean values from two independent experiments shown as individual
1350 data points with two technical replicates each.
1351
1352 **Fig. S2: Replication efficiency of GLT1 compared to Con1 in Huh7 cells, using different**
1353 **replication enhancing conditions.** Huh7 cells were transfected with subgenomic reporter replicons
1354 of the indicated isolates or mutants. Luciferase activity in cell lysates (RLU) was quantified as a
1355 correlate of RNA replication efficiency at the given time points and normalized to 4 h. (**A,C**) HCV
1356 replication was stimulated by SEC14L2 expression compared to empty vector transduction as
1357 indicated. (**B,C**) Replication enhancement of GLT1 (green lines) or Con1 (black lines) by mutations
1358 in NS4B (K1846T), NS5A (S2204R) or NS5B (R2884G). A replication deficient Con1 variant
1359 (Con1ΔGDD) was used as a negative control for replication and the respective luciferase level at
1360 72 h is indicated by a dashed grey line in all diagrams. The data are the mean values from two
1361 independent experiments shown as individual data points with two technical replicates each.
1362
1363 **Fig. S3: Replication efficiency of GLT1 compared to Con1 in Huh7.5 cells, using different**
1364 **replication enhancing conditions.** Huh7.5 cells were transfected with subgenomic reporter
1365 replicons of the indicated isolates or mutants. Luciferase activity in cell lysates (RLU) was
1366 quantified as a correlate of RNA replication efficiency at the given time points and normalized to
1367 4 h. (**A,C**) HCV replication was stimulated by SEC14L2 expression compared to empty vector
1368 transduction as indicated. (**B,C**) Replication enhancement of GLT1 (green lines) or Con1 (black
1369 lines) by mutations in NS4B (K1846T), NS5A (S2204R) or NS5B (R2884G). A replication
1370 deficient Con1 variant (Con1ΔGDD) was used as a negative control for replication and the
1371 respective luciferase level at 72 h is indicated by a dashed grey line in all diagrams. The data are
1372 the mean values from two independent experiments shown as individual data points with two
1373 technical replicates each.
1374
1375 **Fig. S4: Ultrastructural analysis of membrane rearrangements after expression of GLT1**
1376 **NS3-5B NS5A_mCherry and PI4KA activation by different isolates.** Huh7-Lunet T7 cells
1377 either expressing SEC14L2 (T7 SEC14L2) or not (T7 empty) were transfected with a pTM vector
1378 encoding GLT1 NS3-5B with an in frame insertion of mCherry in domain 3 of NS5A (68). Cells

were fixed 24 hours post transfection and the mCherry fluorescent signal was used to identify positive cells for further analysis by CLEM. A minimum of six cells were analyzed and the (**A**) number of DMVs in randomly selected areas and (**B**) the DMV diameter was measured. (**C**) Representative images of each condition. (**D,E**) Huh7-Lunet T7 cells were transfected with plasmids encoding NS3-5B of Con1 WT, GLT1 WT or JFH-1 WT and fixed 24 h post transfection. (D) Total NS5A and PI4P was detected by immunofluorescence analysis using monoclonal antibody 9E10 (red) and anti-PI4P (green), respectively. The nuclei were stained with DAPI. (E) Quantification of the PI4P signal intensity in 71-95 cells using Fiji. Each dot represents one cell. Results shown are mean values from two independent experiments. Unpaired two-tailed Student's t-test was used to determine statistical significance (*** = $p \leq 0.001$).

Fig. S5: Virus production in Huh7.5 cells and analysis of a chimeric GLT1 genome harboring the structural proteins of Con1. (**A**) Detection of intra- and extracellular core protein after transfection of full-length virus genomes. Huh7.5 cells with or without SEC14L2 expression were transfected with the indicated HCV full-length genomes and intra- and extracellular core protein levels were determined by ELISA as correlates of replication and virus secretion, respectively. (**B,C**) A chimeric GLT1 genome, encoding the structural proteins of Con1 up to the C3 junction site in NS2 (24) was transfected in Huh7-Lunet (B) or Huh7-Lunet CD81 (C) cells with or without SEC14L2 expression and/or PCi treatment. Intra- and extracellular core levels were determined by Elisa 72 hours post transfection (B) or before passaging (C). Shown are data from two independent experiments (A, B) or from a single passaging experiment (C). The dashed grey line indicates the detection limit of 3 fmol/l core protein; n.d. = not detectable.

Fig. S6: Input viral titers and analysis of spreading properties of GLT1-20M compared to JC1. (**A**) Viral titer (TCID50/ml) from concentrated supernatant of different HCV isolates harvested from Huh7-Lunet CD81 MAVS-GFP-NLS used in Fig. 4D. (**B,C**) Distribution of the shortest distances between a GLT1-20M (B) or JC1 (C) positive Huh7-Lunet CD81 MAVS-GFP-NLS cell ("donor") and the next nearest Huh7-Lunet CD81 MAVS-mCherry-NLS with nuclear mCherry signal ("recipient") after treatment with HCV neutralizing antibodies or left untreated (mock). Numbers in brackets and vertical lines indicate the median distance for each treatment. Shown are representative data from one experiment (n=2).

Fig. S7: Representative still images from live cell imaging of virus spread assays. Every 30 minutes an image was acquired for 72 hours. Donor cells of interest are labelled with a cyan arrow, recipient cells of interest are labelled with a white arrow. (**A**) Example of cell-to-cell mediated spread in both GLT1cc (Movie S1) and JC1 (Movie S2). (**B-E**) Examples based on JC1 because of the overall higher number of infection events. (**B**) Infection in absence of a visible donor cell representing cell-free spread (Movie S3). (**C**) Cell-to-cell spread with recipient cell moving away from donor cell (Movie S4). (**D**) Vanishing of donor cell after cell-to-cell spread (Movie S5). (**E**) Earliest observed infection event.

1420
1421 **Fig. S8: Identification of polymorphic sequence N2415S in the quasispecies of p118.27 and**
1422 **titer of GLT1cc in Huh7.5 cells.** (A) Sequences of 5 individual subclones of RT-PCR products
1423 obtained from total RNA of p118.27 compared to GLT1-20M. A missing consensus mutation at
1424 position 1074 is shown in blue, premature stop codons are underlined and highlighted in bold.
1425 N2415S is shown in red color. (B) Viral titer (TCID50/ml) from concentrated supernatant of
1426 indicated HCV isolates harvested from Huh7.5 cells; data from two independent biological
1427 replicates.
1428
1429 **Fig. S9: Sequence chromatograms of individual base positions with a shift in abundance in**
1430 **the GLT1-patient serum compared to the mouse serum 8 weeks after infection.**
1431
1432 **Fig. S10: Alternative NS5A domain 1 dimer structures.** The NS5A domain 1 in is anchored to
1433 phospholipid membranes by an N-terminal amphipathic helix (residues 1–33, PDB 1R7G). Crystal
1434 studies revealed four different dimeric forms of domain 1 from genotype 1a and 1b with the same
1435 monomeric unit, but different dimeric arrangements shown. (**A**) The first crystal structure from
1436 genotype 1b (PDB: 1ZH1) with the modelled N-terminal amphipathic helix and the postulated
1437 RNA-binding groove between the two monomers is shown. (**B**) Monomers from genotype 1a (PDB:
1438 4CL1) form a head to head dimer. (**C**) Genotype 1b monomers assemble in parallel to form an
1439 extensive interface (PDB: 3FQM). (**D**) Monomers from genotype 1a dimerize via a similar interface
1440 as shown in C but are assembled in an antiparallel fashion (PDB: 4CL1).
1441

1442 **Movies S1-S5: Live cell imaging of cell spread assay.** Every 30 minutes an image was acquired

1443 for 72 hours. Donor cells were labelled with GFP and recipient cells with mCherry.

1444 **Movie S1: Example of cell-to-cell mediated spread in GLT1cc.**

1445 **Movie S2: Example of cell-to-cell mediated spread in JC1.**

1446 **Movie S3: Infection in absence of a visible donor cell representing cell-free spread in JC1.**

1447 **Movie S4: Cell-to-cell spread with acceptor cell moving away from donor cell in JC1.**

1448 **Movie S5: Vanishing of donor cell after cell-to-cell spread in JC1.**

1449

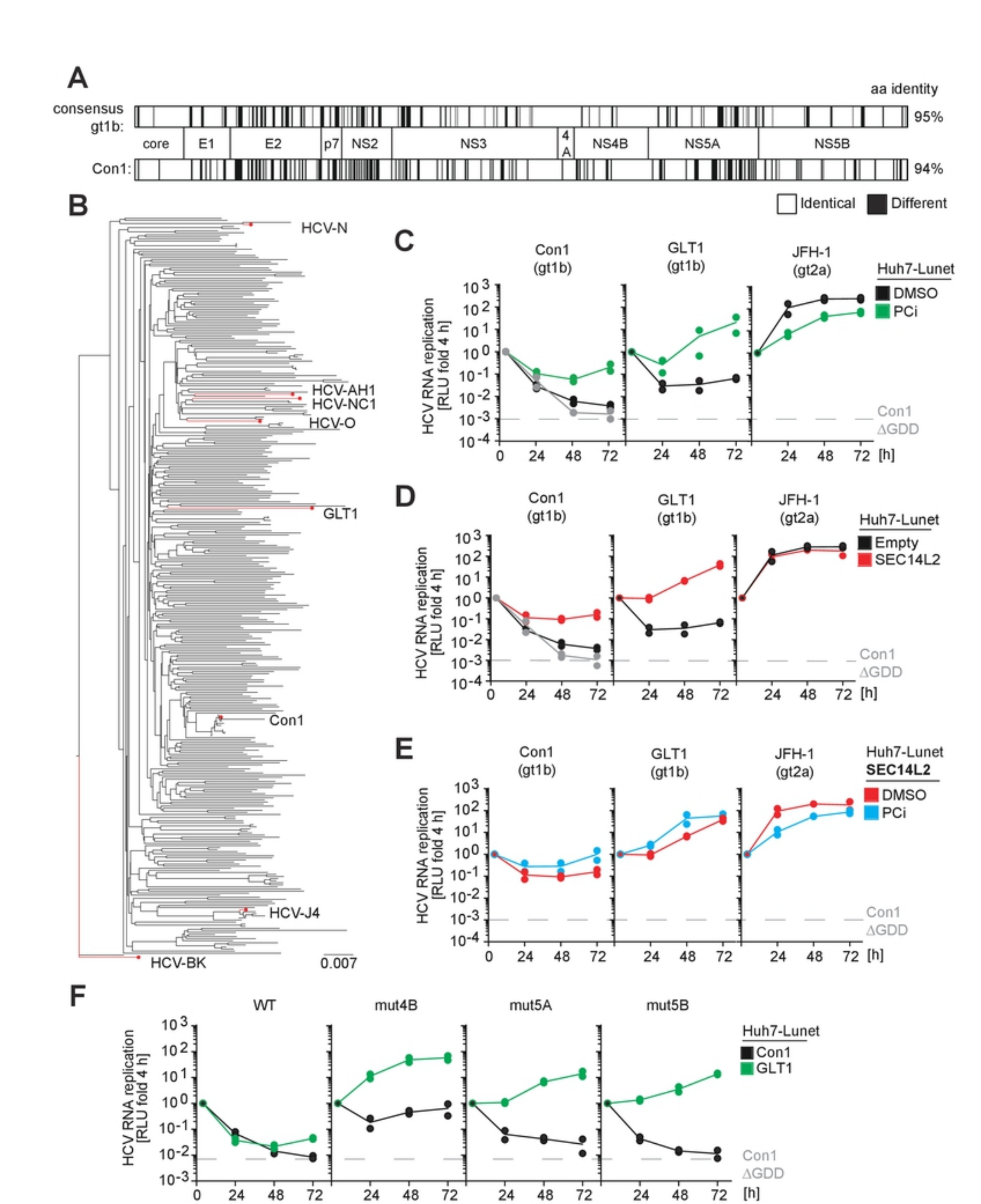
A
aa identity
consensus gt1b:
95%
core
E1
E2
p7
NS2
NS3
4A
NS4B
NS5A
NS5B
Con1:
94%
Identical
Different
B
HCV-N
HCV-AH1
HCV-NC1
HCV-O
GLT1
Con1
HCV-J4
HCV-BK
0.007
C
Con1 (gt1b)
GLT1 (gt1b)
JFH-1 (gt2a)
Huh7-Lunet
DMSO
PCi
HCV RNA replication [RLU fold 4 h]
Con1 ΔGDD
[h]
D
Empty
SEC14L2
E
SEC14L2
F
WT
mut4B
mut5A
mut5B
Con1
GLT1

Figure 1

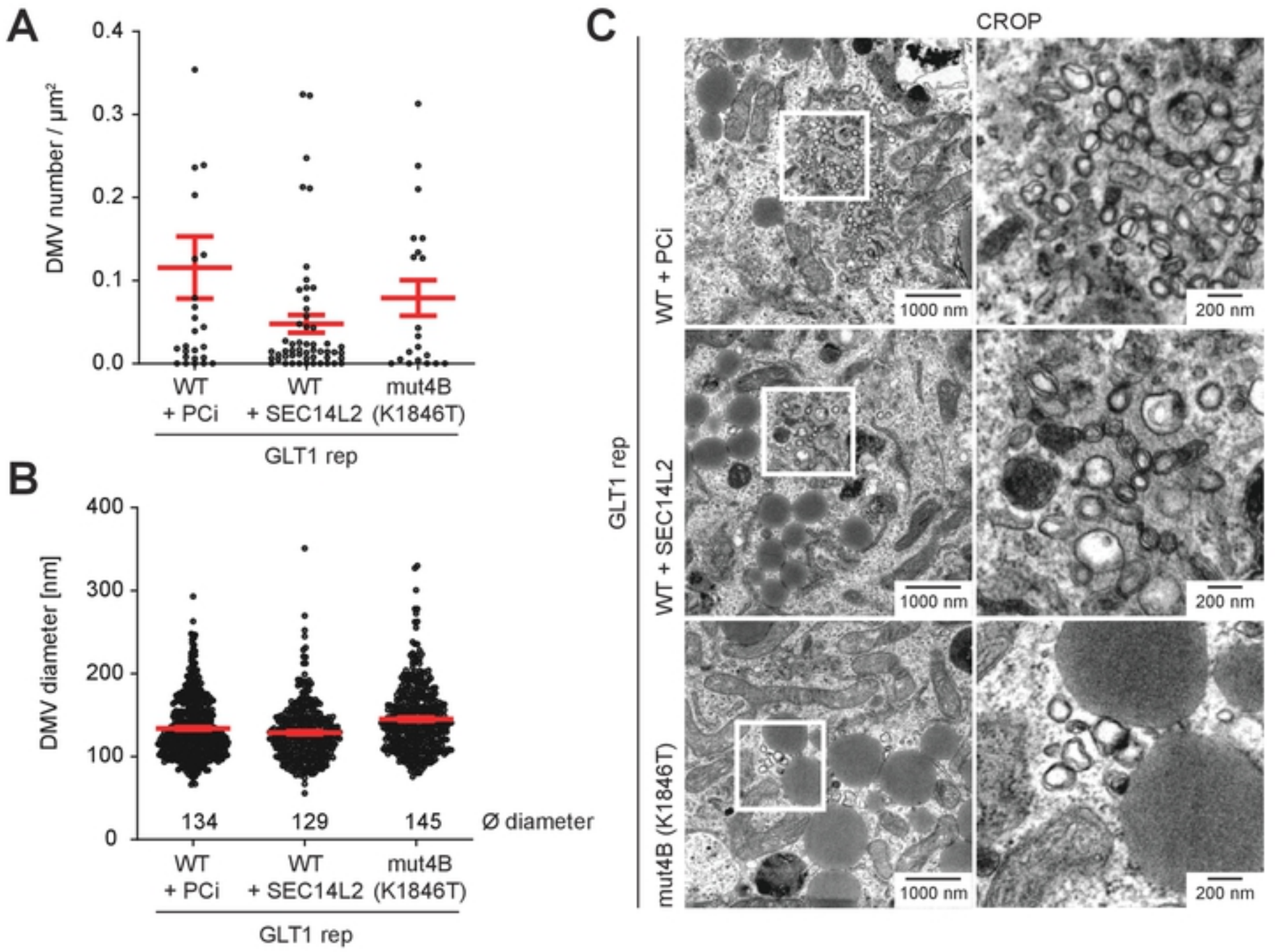
A
DMV number / µm²
0.4
0.3
0.2
0.1
0.0
WT + PCi
WT + SEC14L2
mut4B (K1846T)
GLT1 rep
B
DMV diameter [nm]
400
300
200
100
0
134
129
145
Ø diameter
WT + PCi
WT + SEC14L2
mut4B (K1846T)
GLT1 rep
C
CROP
GLT1 rep
WT + PCi
WT + SEC14L2
mut4B (K1846T)
1000 nm
200 nm

Figure 2

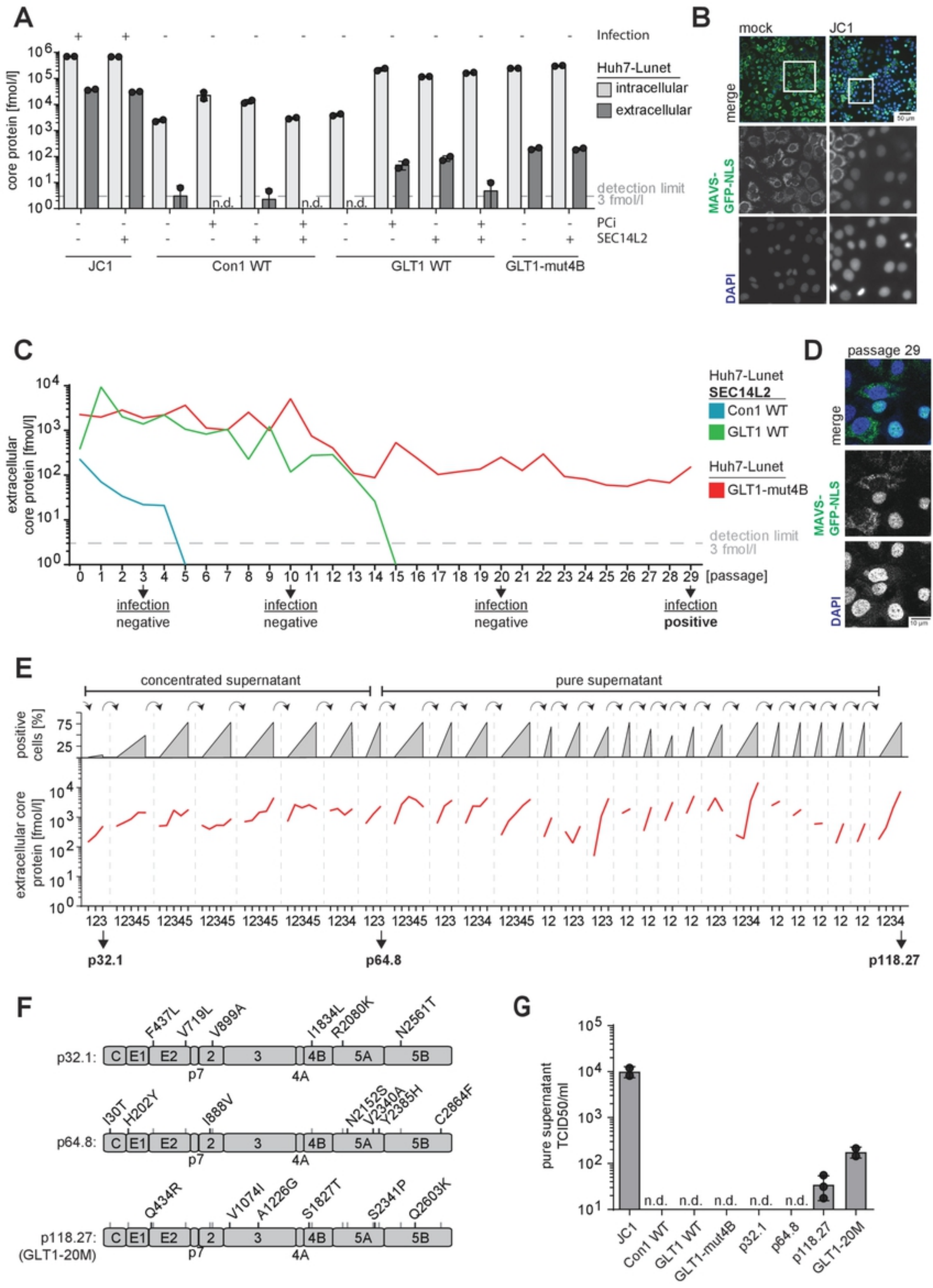
A
Infection
Huh7-Lunet
intracellular
extracellular
core protein [fmol/l]
detection limit
3 fmol/l
n.d.
PCi
SEC14L2
JC1
Con1 WT
GLT1 WT
GLT1-mut4B
B
mock
JC1
merge
MAVS-GFP-NLS
DAPI
C
extracellular core protein [fmol/l]
Huh7-Lunet
SEC14L2
Con1 WT
GLT1 WT
Huh7-Lunet
GLT1-mut4B
detection limit
3 fmol/l
[passage]
infection negative
infection negative
infection negative
infection positive
D
passage 29
merge
MAVS-GFP-NLS
DAPI
E
concentrated supernatant
pure supernatant
positive cells [%]
extracellular core protein [fmol/l]
p32.1
p64.8
p118.27
F
p32.1:
p64.8:
p118.27: (GLT1-20M)
C
E1
E2
p7
2
3
4A
4B
5A
5B
F437L
V719L
V899A
I1834L
R2080K
N2561T
I30T
H202Y
I888V
N2152S
V2340A
Y2385H
C2864F
Q434R
V1074I
A1226G
S1827T
S2341P
Q2603K
G
pure supernatant TCID50/ml
n.d.
JC1
Con1 WT
GLT1 WT
GLT1-mut4B
p32.1
p64.8
p118.27
GLT1-20M

Figure 3

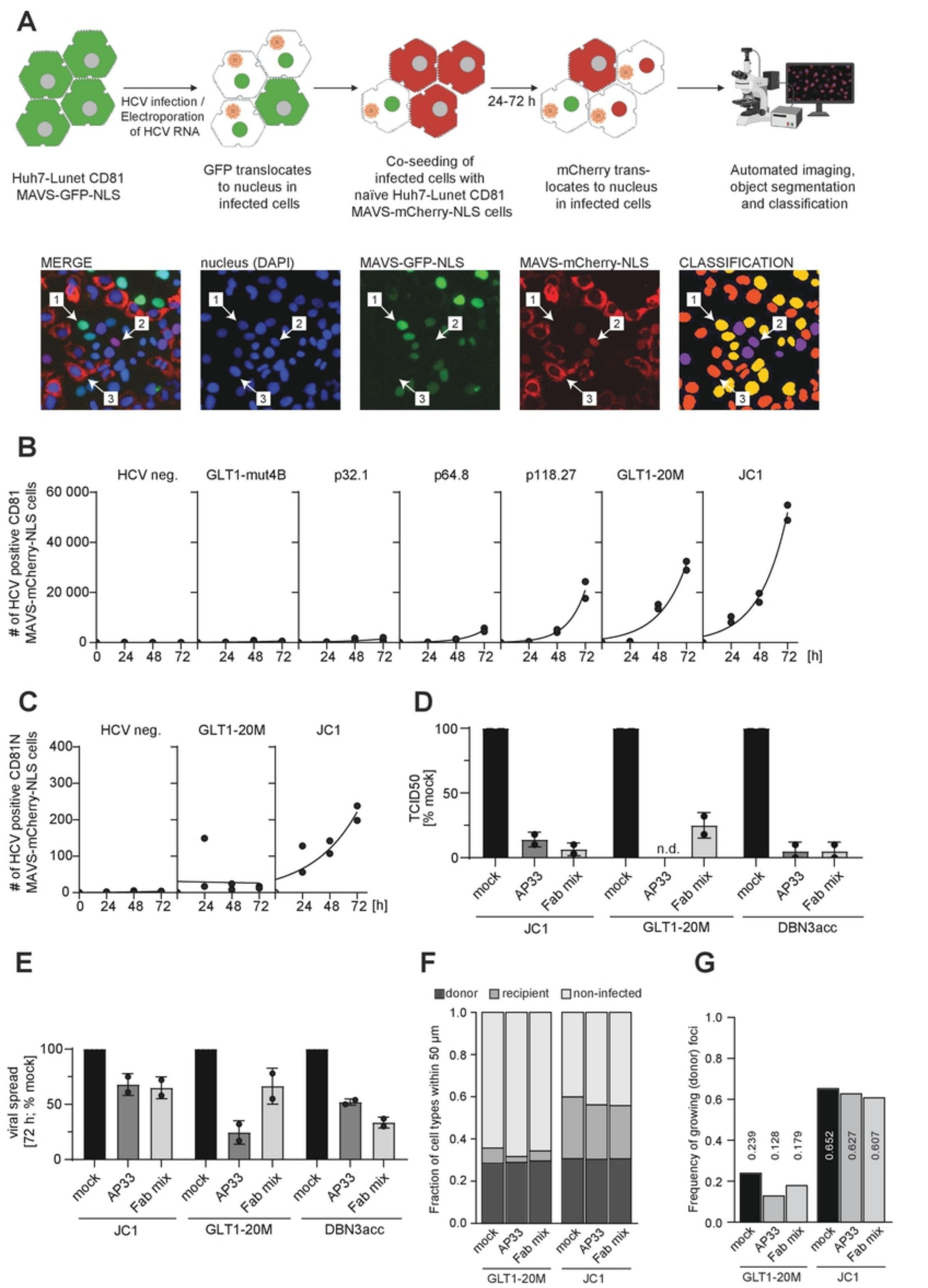
A
HCV infection / Electroporation of HCV RNA
24-72 h
Huh7-Lunet CD81 MAVS-GFP-NLS
GFP translocates to nucleus in infected cells
Co-seeding of infected cells with naïve Huh7-Lunet CD81 MAVS-mCherry-NLS cells
mCherry trans-locates to nucleus in infected cells
Automated imaging, object segmentation and classification
MERGE
nucleus (DAPI)
MAVS-GFP-NLS
MAVS-mCherry-NLS
CLASSIFICATION
B
HCV neg.
GLT1-mut4B
p32.1
p64.8
p118.27
GLT1-20M
JC1
# of HCV positive CD81 MAVS-mCherry-NLS cells
[h]
C
# of HCV positive CD81N MAVS-mCherry-NLS cells
D
TCID50 [% mock]
n.d.
mock
AP33
Fab mix
JC1
GLT1-20M
DBN3acc
E
viral spread [72 h; % mock]
F
donor
recipient
non-infected
Fraction of cell types within 50 µm
G
Frequency of growing (donor) foci
0.239
0.128
0.179
0.652
0.627
0.607

Figure 4

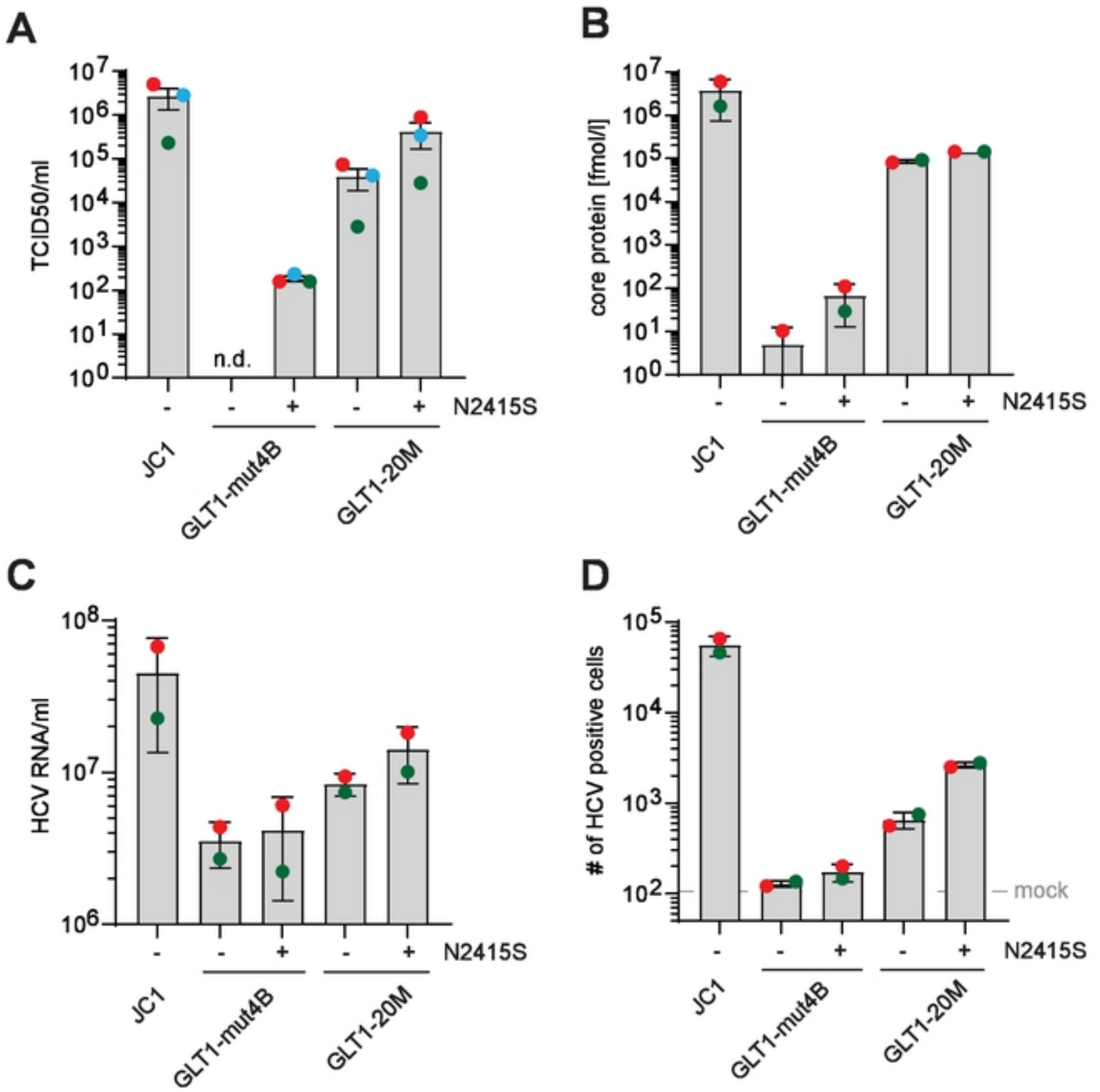
A
TCID50/ml
n.d.
N2415S
JC1
GLT1-mut4B
GLT1-20M
B
core protein [fmol/l]
N2415S
JC1
GLT1-mut4B
GLT1-20M
C
HCV RNA/ml
N2415S
JC1
GLT1-mut4B
GLT1-20M
D
# of HCV positive cells
mock
N2415S
JC1
GLT1-mut4B
GLT1-20M

Figure 5

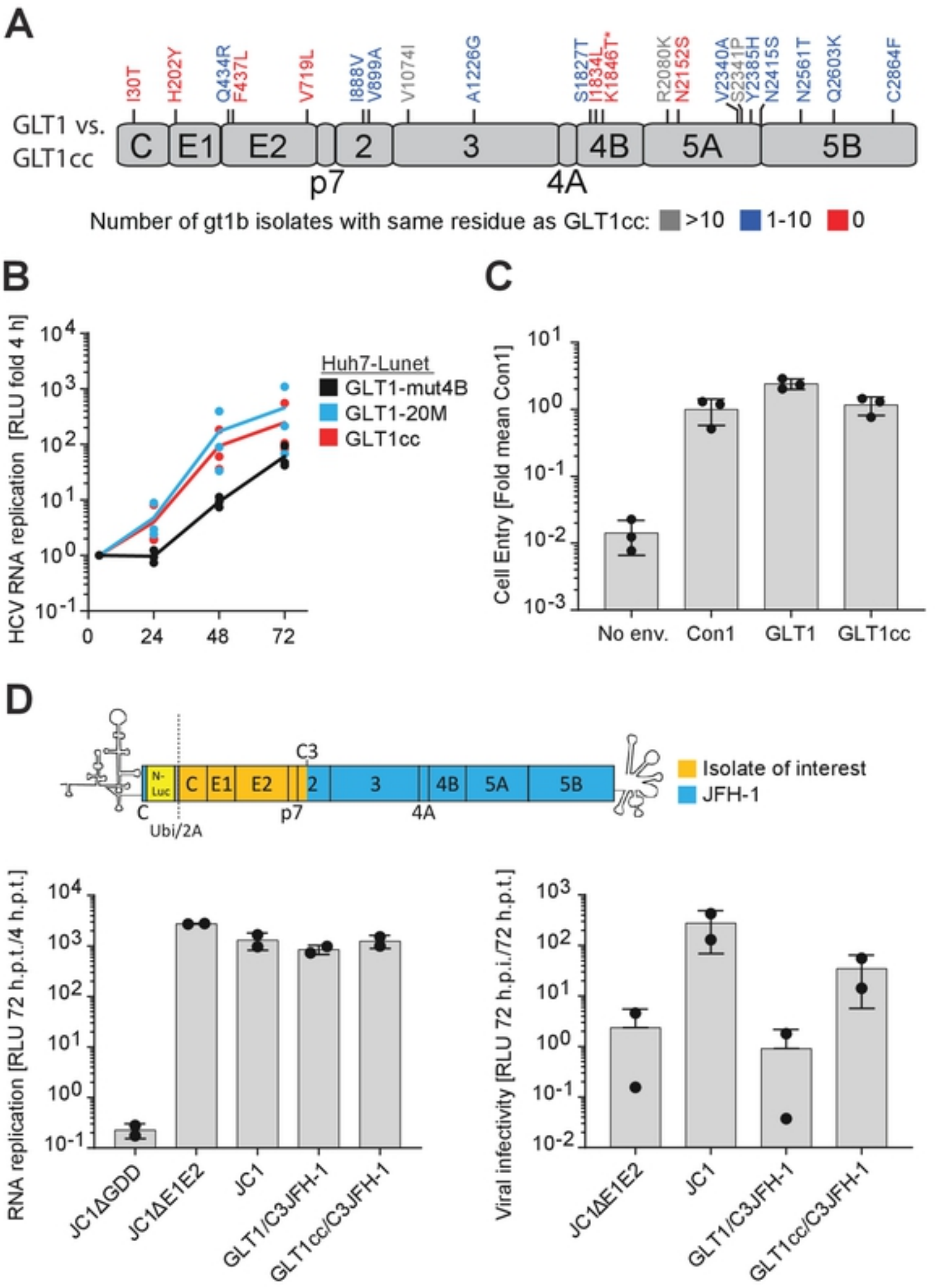
A
I30T
H202Y
Q434R
F437L
V719L
I888V
V899A
V1074I
A1226G
S1827T
I1834L
K1846T*
R2080K
N2152S
V2340A
S2341P
Y2385H
N2415S
N2561T
Q2603K
C2864F
GLT1 vs. GLT1cc
C
E1
E2
p7
2
3
4A
4B
5A
5B
Number of gt1b isolates with same residue as GLT1cc: >10 1-10 0
B
HCV RNA replication [RLU fold 4 h]
Huh7-Lunet
GLT1-mut4B
GLT1-20M
GLT1cc
0
24
48
72
C
Cell Entry [Fold mean Con1]
No env.
Con1
GLT1
GLT1cc
D
N-Luc
C3
Ubi/2A
Isolate of interest
JFH-1
RNA replication [RLU 72 h.p.t./4 h.p.t.]
JC1ΔGDD
JC1ΔE1E2
JC1
GLT1/C3JFH-1
GLT1cc/C3JFH-1
Viral infectivity [RLU 72 h.p.i./72 h.p.t.]

Figure 6

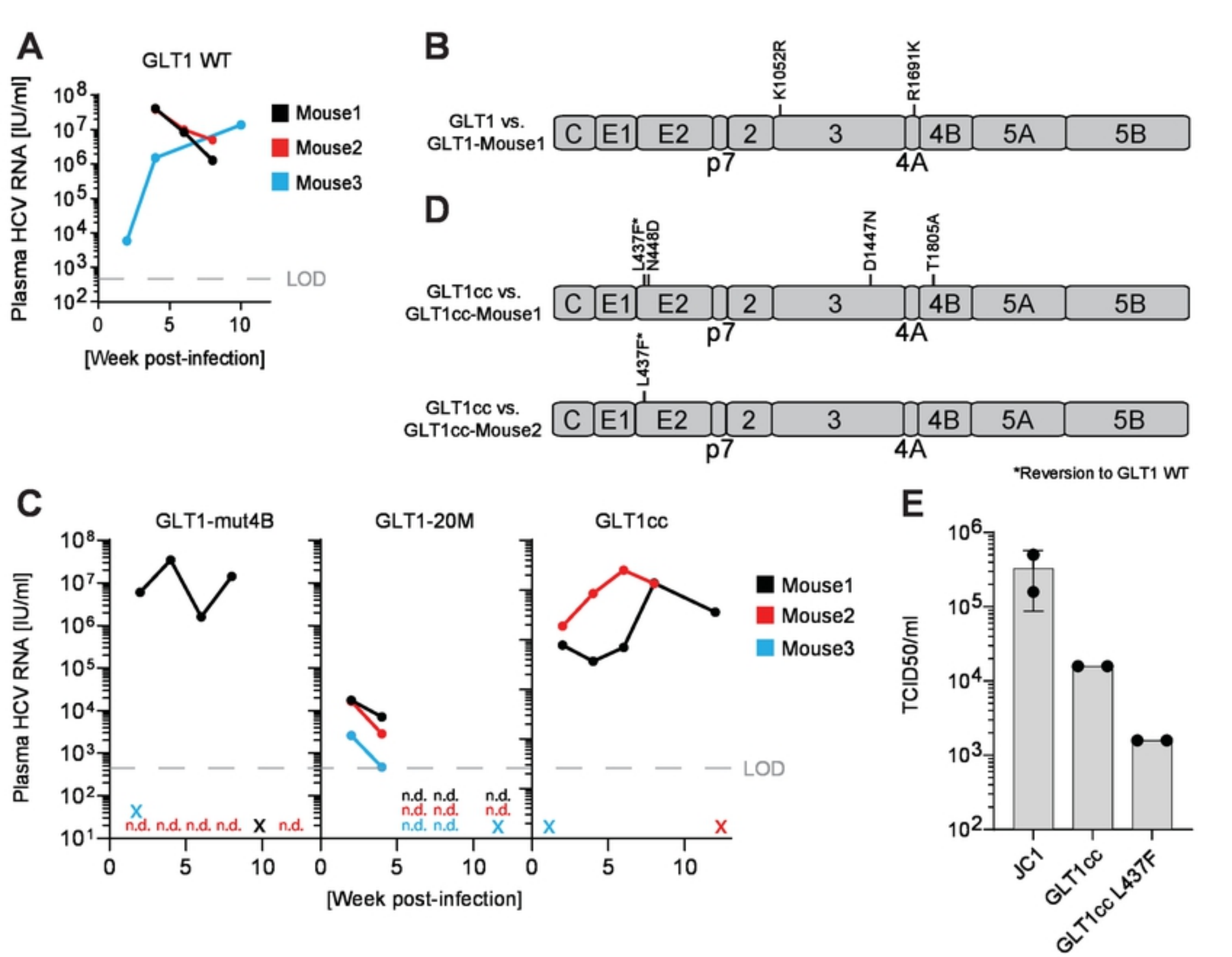
A
GLT1 WT
Plasma HCV RNA [IU/ml]
Mouse1
Mouse2
Mouse3
LOD
[Week post-infection]
B
K1052R
R1691K
GLT1 vs.
GLT1-Mouse1
C
E1
E2
2
3
4B
5A
5B
p7
4A
D
L437F*
N448D
D1447N
T1805A
GLT1cc vs.
GLT1cc-Mouse1
L437F*
GLT1cc vs.
GLT1cc-Mouse2
*Reversion to GLT1 WT
C
GLT1-mut4B
GLT1-20M
GLT1cc
n.d.
E
TCID50/ml
JC1
GLT1cc
GLT1cc L437F

Figure 7

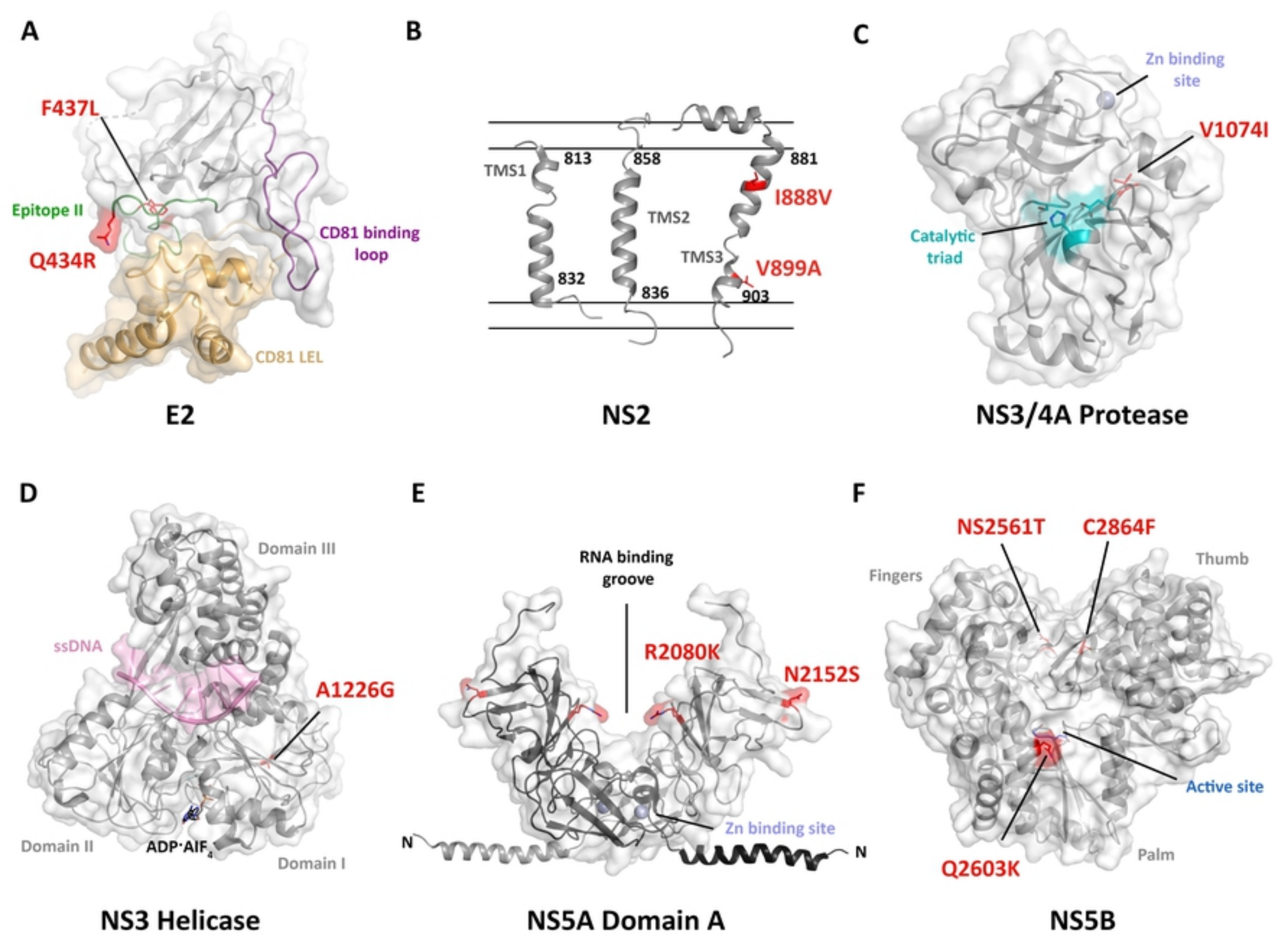
A
F437L
Epitope II
Q434R
CD81 binding loop
CD81 LEL
E2
B
TMS1
813
858
881
I888V
TMS2
TMS3
V899A
832
836
903
NS2
C
Zn binding site
V1074I
Catalytic triad
NS3/4A Protease
D
Domain III
ssDNA
A1226G
Domain II
ADP·AlF4
Domain I
NS3 Helicase
E
RNA binding groove
R2080K
N2152S
Zn binding site
N
N
NS5A Domain A
F
NS2561T
C2864F
Fingers
Thumb
Active site
Q2603K
Palm
NS5B

Figure 8